Title

Development and testing of a mechanistic potential niche model of riparian tree seedling recruitment

Authors

Phillips, Sierra J

Pasternack, Gregory B

Larrieu, Kenneth

Publication Date

2025-02-01

DOI

10.1016/j.ecolmodel.2024.110986

Ecological Modelling 501 (2025) 110986

Contents lists available at ScienceDirect

Ecological Modelling

journal homepage: www.elsevier.com/locate/ecolmodel

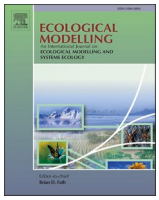

Development and testing of a mechanistic potential niche model of riparian tree seedling recruitment

Sierra J. Phillips [a,*], Gregory B. Pasternack [a], Kenneth Larrieu [b]

[a] Department of Land, Air, and Water Resources, University of California, Davis, One Shields Avenue, Davis, CA 95616, USA
[b] Department of Civil and Environmental Engineering, University of California, Davis, One Shields Avenue, Davis, CA 95616, USA

ARTICLE INFO

Keywords:
Seedling recruitment
Habitat suitability
Hydrophysical processes
Ecohydraulics
Potential niche model
Mechanistic model
Riparian vegetation

ABSTRACT

Seedling recruitment is an important reproductive process for sustaining riparian tree populations in arid and semi-arid environments. Riparian tree species such as cottonwoods and willows are highly adapted to the dynamic riparian environment; their seed dispersal and germination patterns are tied with climatic signals that also drive hydrology. The magnitude and timing of seasonal hydrologic components determine environmental conditions that either promote or limit seedling establishment processes. This article presents the development and testing of a potential niche model for riparian seedling recruitment. The presented Riparian Seedling Recruitment Model (RSRM) identifies spatially explicit locations of suitable habitat for seedling recruitment driven by relevant hydrophysical processes. This model extends previous seedling recruitment algorithms by accounting for seedling mortality due to scour by sediment mobilization, the reduction of potential germination sites due to existing forest canopy shade, and the incorporation of engineered channel and substrate modifications. The model is integrated into the open-source river analysis software River Architect. Potential future applications for the model include assessing seedling recruitment patterns for existing conditions, under alternative flow regimes, or for designs with topographic modifications. A canonical test channel and five scenarios with relevant hydrographic features are used to perform an implementation verification. Predictable recruitment patterns for the canonical test channel demonstrate model functionality and establish a dataset for future benchmarking. Finally, results from a site on the lower Yuba River, California are presented to illustrate the usefulness of a simplified test site given the complexity of results from real-world data.

1. Introduction

Cottonwoods (*Populus* spp.) and willows (*Salix* spp.) are keystone riparian species across the temperate Northern Hemisphere (Cooke & Rood, 2007). As pioneer species, they rapidly colonize disturbed or newly formed landforms, playing essential roles in ecosystem dynamics (Holstein, 1984; Stromberg, 1993). In dynamic systems like rivers, species must adapt continuously to survive and reproduce, as the availability and quality of habitat varies spatially and temporally (Stanford et al., 2005).

Seedling recruitment consists of three processes: germination, survival, and growth (Eriksson & Ehrlén, 2008; Ribbens et al., 1994). Successful cottonwood and willow seedling recruitment is episodic due to climatic and hydrologic fluctuations, resulting in interannual variability of recruitment (Baker, 1990; Johnson, 1994; Mahoney & Rood, 1998; Rood & Mahoney, 1990; Stella et al., 2006). The sensitivity and timing of seedling recruitment requirements create a demographic bottleneck at the seedling recruitment stage resulting in extensive seedling recruitment occurring on a 5- to 50-year cycle depending on the system (Cooper et al., 2003; Lytle & Merritt, 2004; Philipsen et al., 2021; Scott et al., 1996; Scott & Miller, 2017; Shafroth et al., 1998; Stromberg et al., 1991). Prolific recruitment years often follow disturbance events, such as ice, wildfire, or flood, which create new suitable habitats for germination (Lytle & Merritt, 2004; Rood et al., 2007).

Riparian forests dominated by pioneer tree species have been impacted by land use conversion, disease, drought, and modification of disturbance regimes and stressors (Nilsson & Berggren, 2000; Stella & Bendix, 2019). Dams disrupt the natural flow and sediment regimes. Fragmentation of river corridors by dams alters the patterns of disturbance events and physical stressors outside of the normal ranges to which riparian species have adapted (Poff, 1997). Flow regulation can impede seedling recruitment of riparian trees via decoupling of

* Corresponding author.
E-mail address: sjphillips@ucdavis.edu (S.J. Phillips).

https://doi.org/10.1016/j.ecolmodel.2024.110986
Received 21 June 2024; Received in revised form 4 December 2024; Accepted 5 December 2024
Available online 4 January 2025

snowmelt-driven flow peaks with seed release, and reducing rates of channel migration, a process that forms new barren areas for pioneer establishment (Johnson, 1994, 2000; Perry et al., 2020). Flow regulation and drought have altered riparian forest structure and resulted in reduced forest abundance or complete collapse in rivers, such as the Missouri River (Dixon et al., 2012), Rio Grande (Howe & Knopf, 1991), Green River (Cooper et al., 1999), Santa Clara River (Williams et al., 2022), and St. Mary River and Waterton River in Canada (Rood & Heinze-Milne, 1989). The causes of the decline of riparian forests can be attributed to an increase in adult mortality and a decrease in the frequency of prolific recruitment events. Not all regulated rivers have seen a decline of riparian forests after damming, with recent examples on the South Platte River (Christensen et al., 2023) and Red Deer River, Canada (Philipsen & Rood, 2022). In these systems, the rivers still experience inter-annual flow variability including peak flood events that drive geomorphic disturbance events which effectively promote seedling recruitment.

Understanding the mechanisms driving the presently ongoing decline of seedling recruitment remains a difficult challenge for river managers and restoration practitioners, let alone predicting future scenarios. As demonstrated for other linked abiotic-biotic environmental phenomena, it is conjectured that a combination of hydrophysical processes drive the environmental conditions that in turn determine the suitability of a location for seedling recruitment. Consequently, modeling these processes can be used to predict recruitment potential.

The following section provides a review of the methods of a new mechanistic model that predicts the spatial distribution of suitable sites for riparian seedling recruitment. The method presented herein is like previous approaches (Benjankar et al., 2014, 2020; Tranmer et al., 2023) but with notable improvements. The model's implementation of the mathematical representations is described in the methods. Next, the method for verifying the implementation of the model is accomplished with a canonical test channel and five scenarios, each representing a different combination of important hydrologic features in their flow records that should lead to predictable recruitment potential patterns given the model's key assumptions. Finally, the results from a site on the lower Yuba River in California are shown to illustrate the usefulness of a simplified test site given the complexity of results from real-world data. Additionally, the source code is provided on GitHub (https://riverarchitect.github.io/) as a new module in the open-source River Architect software, which has other automated ecohydraulic analysis and river design assessment tools that have been previously published (Schwindt et al., 2020). This makes the analytical method reproducible and predictive modeling accessible to non-coders. Potential uses of the tool include identifying the relative importance of processes in driving recruitment in a system to inform the schedule of flows in regulated rivers or aid in restoration project design.

2. Riparian Seedling Recruitment Model (RSRM)

The Riparian Seedling Recruitment Model (RSRM) simulates the availability of the potential seedling recruitment niche for a given terrain, species of interest, and flow record (Fig. 1). It is a plan-view, spatially explicit 2D (two-dimensional) grid model.

2.1. Model conceptualization

The new model presented herein builds on existing conceptual and applied models that aimed to quantify the spatial distribution of the potential for seedling recruitment beginning with the 'recruitment box' model. The 'recruitment box' is a conceptual model describing how site hydrology, seed dispersal, and drought tolerance influence successful cottonwood seedling recruitment (Mahoney & Rood, 1998). While the model was originally conceptualized for cottonwood trees, it has been successfully applied to evaluate other riparian trees and shrubs that have similar seedling recruitment patterns.

Model conceptualization begins with defining where riparian woody species seedlings successfully establish and survive their first year of life. By considering dispersal limitations and physiological tolerances, it is assumed that the RSRM is modeling the recruitment niche where seedling recruitment will successfully occur making the model a mechanistic 'potential niche model' (Sillero, 2011). Each requirement for the creation of suitable seedling recruitment sites is related to a hydrophysical process driven by seasonal hydrologic component (Table 1). These hydrophysical processes have been previously defined and used to evaluate cottonwood seedling recruitment in past studies (Benjankar et al., 2014; Braatne et al., 2007; Burke et al., 2009), so a detailed description of how the RSRM numerically represents them is provided to highlight the differences in our approach.

Hydrophysical processes are assumed to be the controlling factors on seedling recruitment. Stochasticity and biotic factors like herbivory, pests, and disease are not considered, which may result in

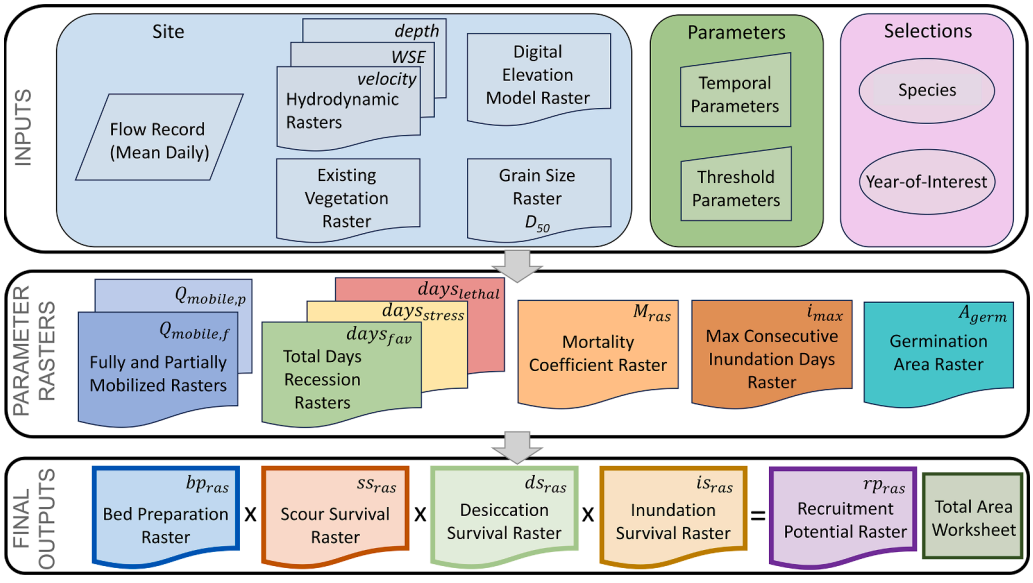

Fig. 1. Conceptual diagram of the Riparian Seedling Recruitment Model (RSRM) including the required model inputs, the recruitment parameter rasters calculated to numerically represent each hydrophysical process, and the final raster outputs.

Table 1
Hydrophysical processes defined by a seasonal hydrologic component and conditions for seedling recruitment.

Hydrophysical process	Seasonal hydrologic component	Conditions for seedling recruitment
Bed preparation	Peak winter flow prior to germination	Mechanical disturbance removes young existing vegetation creating bare surface needed for a germination site
Establishment	Spring streamflow recession	Moist substrate required to support germination
Recession	Streamflow recession until baseflow conditions begin	Roots must maintain contact with receding riparian water table
Prolonged inundation	High flows during winter and spring after establishment	Seedlings are intolerant to having their roots or stem/leaves underwater for prolonged period
Scour after establishment	Peak winter and spring flows after establishment	Seedlings are susceptible to uprooting

overprediction of potential suitable recruitment sites. Abiotic processes such as air and water temperature, antecedent soil moisture, or precipitation are not considered in a mechanistic way such as degree-days being used to determine the seed dispersal period or water temperature stressing seedlings. Competition between plant species is not considered given that vegetative competition is not a limiting factor for seedling recruitment in the first year (Stella, 2005).

The RSRM evaluates five hydrophysical processes to determine the suitability of a site for seedling recruitment. These include (1) bed preparation, (2) establishment, (3) recession, (4) prolonged inundation, and (5) scour after establishment. These processes are assumed to be independent from one another. For example, seeds that settle onto the riverbed and begin to germinate do not drive or influence recession. Each hydrophysical process is numerically represented by mechanistic rules that relate seed dispersal phenology, seed and seedling physiological tolerances, and hydraulic conditions. Hydrodynamic simulation results allow for the numerical representation of these processes by calculating the critical flow necessary for mobilizing sediment with modeled depths and velocities and using interpolated water surface elevations to track inundation or the approximate depth of the riparian water table (Table 2).

2.2. Temporal analysis periods

Each process or life stage event has an associated temporal period during which the event must occur, as the timing is crucial due to limitations, such as seed dispersal and viability and seedling root growth. Five temporal periods associated with important hydrophysical processes are considered to evaluate seedling recruitment (Fig. 2). The five temporal periods are not completely distinct; two or more processes can

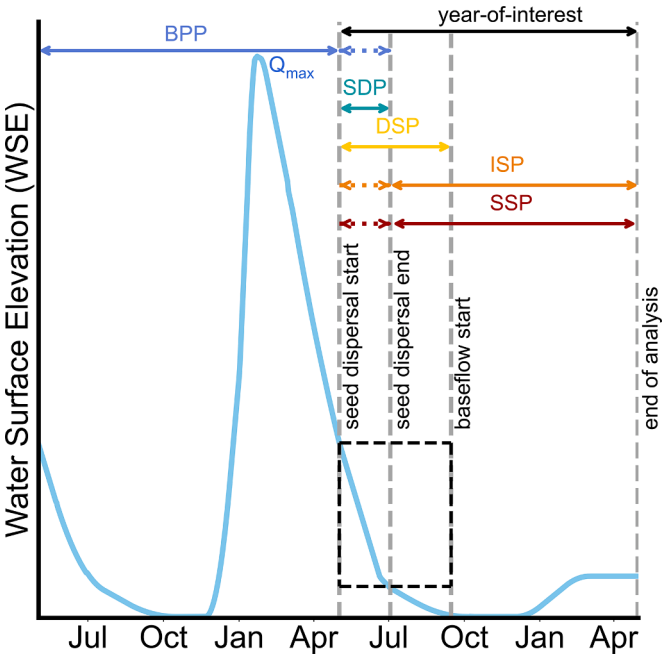

Fig. 2. Hydrograph showing the recruitment box and temporal periods associated with the important hydrophysical processes for seedling recruitment (BPP = bed preparation period, SDP = seed dispersal period, DSP = desiccation survival period, ISP = inundation survival period, SSP = scour survival period). Dashed lines show the time a period may be extended into, and solid lines show the period that will be analyzed.

operate concurrently, so overlap exists among the periods. The bed preparation period evaluates flows in the years prior to a selected year of interest during which a site can be expected to remain barren after a peak flood event. This period may include a part of the seed dispersal period, if a sediment mobilizing flow occurs after seeds begin to release (Fig. 2).

The recruitment box boundaries are set by the timing of seed dispersal and the corresponding elevations where successful seedling recruitment is likely (Mahoney & Rood, 1998). The recruitment band is defined as the elevations where establishment and survival are likely caused by a combination of root growth and capillary fringe extent. Mahoney and Rood (1998) say that the seed-release period and recruitment band are used to define the boundaries of the recruitment box zone where seedlings are likely to recruit and survive desiccation stress, which defines a survivable rate of stage decline.

The seed dispersal period should encompass the seed release period and the length of seed viability. Potential germination is only considered during the seed dispersal period if a grid cell has gone dry to represent

Table 2
Numerical representation and equations used to model each hydrophysical process.

Hydrophysical process	Numerical representation	Calculated metric
Bed preparation	Highest flow during bed preparation period ($Q_{max,b}$) flow required to exceed critical bed shear stress threshold at a cell (Q_{mobile})	Cell is prepared if $Q_{max,b} \geq Q_{mobile}$
Establishment	Water surface elevations (WSE) during seed dispersal period are interpolated between modeled flows ($\widetilde{WSE}$) and extended ($\widetilde{WSE}_e$) and compared to the topography (DEM)	Cell is suitable for germination if $\widetilde{WSE}_e > DEM$ (wetted) then $\widetilde{WSE}_e < DEM$ (dry)
Recession	3-day moving average of recession rate (r) at a cell recorded and used to calculate mortality coefficient (M)	$r = \frac{\widetilde{WSE}_{e,-3} - \widetilde{WSE}_e}{3}$ $M = \frac{(\%days_{lethal} \times 3) + (\%days_{stress} \times 1)}{3}$
Prolonged inundation	Consecutive days of inundation (i) at a cell tracked	Number of days that $\widetilde{WSE}_e > DEM$
Scour after establishment	Highest flow after establishment ($Q_{max,s}$) flow required to exceed critical shear stress threshold at a cell (Q_{mobile}) stress threshold	Cell is disturbed if $Q_{max,s} \geq Q_{mobile}$

the risk of seeds being washed away from a given cell if it is inundated. The last day in the seed dispersal period where a cell has gone dry is when desiccation and prolonged inundation survival tracking begins to simulate the start of the process of a viable seed finding a suitable moistened site and germinating. This results in the variable seed dispersal period end and start dates (on a cell-by-cell basis) and modifies the bed preparation and inundation survival periods (Fig. 2). This novel approach significantly impacts how the mortality coefficient is calculated. The total days of the desiccation survival period is adjusted based on when germination would start on a cell-by-cell basis, which is the denominator variable in the mortality coefficient equation.

Four temporal recruitment parameters defining the important temporal analysis periods must be selected based on the species, site, and the patterns of the daily flow record (Table 3). The four parameters include: (i) seed dispersal period start, (ii) seed dispersal period end, (iii) bed preparation period length, and (iv) baseflow period start.

2.3. 2D steady state hydrodynamic modelling

The RSRM utilizes a raster digital elevation model (DEM) and steady-state 2D hydrodynamic model output rasters corresponding to the range of flows observed during the analysis period in order to approximate the hydraulics that drive sediment mobilization, inundation, and riparian water table levels. Any 2D hydrodynamic model can be used, but to model the relevant hydrophysical processes for a given scenario, the RSRM requires depth, WSE, and velocity magnitude rasters for each discharge. If a non-rectangular mesh-based 2D hydrodynamic model is used (e.g., SRH-2D), then model outputs must be converted to raster format.

The RSRM requires depth, WSE, and velocity magnitude rasters of five discharges at a minimum, though several more are highly recommended. The five essential discharges to be simulated include (i) lowest and (ii) highest observed during the analysis period, (iii) highest during the bed preparation period ($Q_{max,b}$), (iv) highest after establishment ($Q_{max,s}$), and (v) lowest during seed dispersal period. Peak discharges during the bed preparation period and after establishment should be modeled exactly as there is no interpolation or extrapolation of dimensionless bed shear stress rasters possible to represent the sediment mobilization during these events. If the exact discharge is not modeled, the depth and velocity rasters of the closest discharge that is less than the peak discharge in the flow record will be used to approximate preparation or scouring of an area. Other model discharges can be determined by reviewing where the slope of the stage-discharge rating curve changes considerably, as the model uses a piecewise linear function.

2.4. Bed preparation and scour analysis

Peak flood flow is modeled to simulate the disturbance that potentially mobilizes sediments during the bed preparation period and after establishment. To determine if the bed has been adequately prepared for the germination of cottonwood seeds, shear stress is used to predict the spatial distribution of sediment mobilization and subsequent removal of young, small vegetation at different discharges. For this analysis, local scour caused by bar-scale sediment transport (Type IIb) was selected, as stem-related vortices scour is only relevant at shallow depths of less than or equal to 0.024 meters (Bywater-Reyes et al., 2015; Edmaier et al., 2011).

Grain mobilization is predicted as a function of dimensionless bed shear stress (τ_*) by selecting a critical threshold value (τ_{*cr}) for motion (Du Boys, 1879; Kramer, 1932; Von Karmàn, 1930). Dimensionless bed shear stress was calculated with the following equation in River Architect (Einstein, 1950; Keulegan, 1938; Schwindt et al., 2019):

$$\tau_* = \frac{1}{D_{84}g(s-1)}\left[\frac{u}{5.75log_{10}(12.2h/(2D_{84}))}\right]^2 \quad (1)$$

where D_{84} is the grain diameter approximated as $D_{84} = 2.2D_{50}$ (Rickenmann & Recking, 2011), g is the gravitational acceleration (9.81 m/s^2), s is sediment grain and water density ratio (2.68 g/cm^3), u is water velocity (m/s), and h is depth (m). This method allows for a spatially distributed grain size raster to be input rather than a single representative grain size for the entire area. The bed preparation analysis creates a set of dimensionless bed shear stress (τ_*) rasters for each modeled discharge.

The partially and fully mobilized flow rasters ($Q_{mobile,p}$, $Q_{mobile,f}$) identify the flow where the τ_* is greater than or equal to the τ_{*cr} for each of those sediment transport regimes (Lamb et al., 2008; Pasternack, 2011; Shields, 1936). A value is assigned to each cell that represents the flow necessary for full or partial mobilization (Table 4). The peak flow during the bed preparation period ($Q_{max,p}$) is then determined and compared to both sets of mobilized flow rasters. There is an option to consider how bed preparation will be modified if an area has recently been disturbed by artificial grading activity. Grain size is considered by including a threshold grain size (D_{cr}) value that captures substrate that is too large to be a suitable site for germination. A graded area extent can be defined wherein if the grain size (D_{50}) is less than the grain size threshold (D_{cr}) the area is considered fully prepared, as it is assumed that the grading would remove vegetation and create a suitable site for germination that mimics the bed preparation process.

Scour is analyzed using the same methodology as for bed preparation as a way of determining if a newly established seedling will experience scour-induced uprooting. The site being undisturbed is favorable for seedling survival during the scour and survival period in contrast to

Table 3
Temporal recruitment parameters of the RSRM with their respective significance and recommendations for how to determine the parameter values.

Temporal parameter	Significance	Recommendation
1. Seed dispersal period (DOY - DOY)	Cells that are wet then dry during this period represent the germination area	Species and site specific decision
2. Bed preparation period (years)	Maximum flow (Q_{max}) during period will determine bed preparation	Species and site specific decision
3. Baseflow period start (DOY)	End of desiccation and prolonged inundation period	Determined from daily flow record

Table 4
Threshold recruitment parameters of the RSRM and the calculations they are used for to determine the condition created by the hydrophysical process modeled.

Threshold parameter	Equation	Units	Calculation	Raster
Critical dimensionless bed shear stresses (τ_{*cr})	1	-		
Fully mobilized (τ_{*f})			$\tau_* \geq \tau_{*f}$	$Q_{mobile,f}$
Partially mobilized (τ_{*p})			$\tau_{*p} \leq \tau_* < \tau_{*f}$	$Q_{mobile,p}$
Bed preparation threshold[1]	-	mm		
Grain size (D_{cr})			$D_{50} \leq D_{cr}$	bp_{ras}
Recession rate (r_{cr})	2	cm/day		
Stressful rate (r_s)			$r_s \leq r < r_L$	d_{stress}
Lethal rate (r_L)			$r \geq r_L$	d_{lethal}
Prolonged inundation (i_{cr})	-	days		
Stressful inundation (i_s)			$i_s \leq i \leq i_L$	is_{ras}
Lethal inundation (i_L)			$i > i_L$	
Recruitment band elevation[2] (b_{cr})	-	cm		
Lower elevation (b_L)			$b \geq b_{*L}$	A_{germ}
Upper elevation (b_u)			$b \leq b_{*u}$	

[1] Optional parameter to set grain size threshold, see 2.4 Bed preparation and scour analysis.
[2] Optional parameter to set recruitment band elevations, see 2.6 Germination area delineation.

disturbance (i.e., sediment mobilization) being favorable for the bed preparation period. Type I uprooting is more relevant to newly established seedlings due to their shallow roots providing little resistance to drag forces, so after seedling survives their first year of life they are not as susceptible to Type I uprooting due to the development of root system (Edmaier et al., 2011).

Partial or complete burial can also cause stress and mortality. This process is highly dependent on plant height and burial depth. Cottonwood seedlings have been found to survive when a significant portion of their stem is exposed (Kui & Stella, 2016). Without a multidimensional morphodynamic model to predict sediment deposition spatially, the RSRM is unable to reasonably evaluate where burial will occur. Some studies have found associations between low τ_* values and deposition (e.g., Li & Pasternack, 2023; Sawyer et al., 2010), but there is insufficient evidence to assume that. This is a complex process to include due to the non-linear effects that burial has on seedling survival and growth as complete burial has been found to kill all cottonwood seedlings, partial burial can be beneficial resulting in increased height and canopy expansion (Kui & Stella, 2016). Ultimately, scour and deposition are both a threat to newly established seedlings, so future developments to the model could include burial depth estimation.

2.5. Water surface elevation linear interpolation

Water surface elevation rasters are required for evaluating the germination area, desiccation survival, and prolonged inundation survival in a defined area. A 2D model outputs the WSE for only the contiguous wetted area of a river. If only depth rasters are available, the model will calculate *WSE* rasters as the sum of the depth raster and DEM. The RSRM uses a pre-existing algorithm in River Architect (Larrieu et al., 2021) to compute a WSE_e raster, defined as a spatial interpolation of the *WSE* raster across the wider river corridor. The WSE_e raster inundates disconnected, low-elevation landforms and provides water table depths for recession analysis. Further details about the spatial interpolation methods are presented in the Supplementary Materials file.

The RSRM allows users to analyze mean daily flow records without the need to model every flow in the record. The two nearest flows with WSE_e rasters (Q_1, Q_2) are used to calculate a WSE_e array for the unmodeled flows ($\widetilde{Q}$) using linear interpolation. The model may fail to accurately interpolate the WSE_e between modeled flows if the stage change is too large between subsequent discharges.

2.6. Germination area delineation

The RSRM presents an alternative way of defining the germination area that does not depend on the definition of recruitment band elevations as previous models have required (e.g., Benjankar et al., 2014, 2020; Burke et al., 2009; Tranmer et al., 2023). The germination area (and thus the area cropping all other analyses in the model) is set by the extent of wetted area between the highest and lowest flows during the seed dispersal period to provide an approximation of the area that is moistened while viable seeds are being dispersed. This modifies the recruitment box so that the left and right boundaries of the box are the beginning of seed release and the beginning of the baseflow period, respectively. This allows for the stress caused by recession to be evaluated throughout the entire growing season rather than just the seed dispersal period (Fig. 2). The temporal recruitment parameters that will set the upper and lower boundaries of the germination area extents are the seed dispersal start and end dates (Table 3). These wetted extent rasters area calculated by subtracting the DEM from the WSE_e, which may not produce the same extents as the wetted area of the depth rasters would produce due to the interpolation method.

If a user would like to apply the recruitment band method and assess recession rates only during the seed dispersal period, the recruitment elevation band parameters (b_{*cr}) values can be defined (Table 4). In that case, the start of baseflow conditions should be set to the same day-of-year (DOY) as the end of seed dispersal. The start and end of seed dispersal is set by the user as a DOY and should be informed by the observed seed dispersal patterns for a given species of interest in the area being analyzed.

2.7. Effects of established vegetation

Seeds are not likely to germinate where vegetation stems already exist, nor are they likely to be successful close to a much larger stem under the canopy of that plant or patch of plants (Harris, 1987; Read, 1958; Rood et al., 1998; Scott et al., 1996; Shafroth et al., 1995; Strahan, 1984). To account for the effects of existing vegetation, a raster representing the canopy extents of existing vegetation can be input to designate areas where established vegetation is not expected to be uprooted by local scour and removes this area from the potential germination area (A_{germ}). Deciding which vegetation to include depends on factors such as the type and size of vegetation, the presence of armoring, and material cohesion. Additionally, it is recommended that 2D hydrodynamic modeling accounts for spatially distributed vegetation roughness (Abu-Aly et al., 2014) to simulate the effects of vegetation on hydraulics more accurately.

2.8. Recession rate analysis

Recession rate is calculated by comparing the interpolated $\widetilde{WSE}_e$ rasters to the ground surface elevation (DEM) on a cell-by-cell basis for each day. When $\widetilde{WSE}_e <$ DEM the elevation of the $\widetilde{WSE}_e$ approximates the riparian water table, assuming that the riparian water table can be interpolated from WSE. This assumption is made in rivers with coarse substrate where it would be expected that little capillary capacity is present (Mahoney & Rood, 1998) and no confining cohesive layer sustains a higher water table locally. If capillary fringe is expected to influence the riparian water table, the user should consider adjusting site-specific recession rate parameters to account for this. If recession is too fast, seedlings roots will not be able to maintain contact with the riparian water table. Stressful (r_s) and lethal (r_L) recession rate thresholds parameters are defined by the user based on site and species specific data, which are expected to exceed the rate of root growth.

A 3-day moving average (r) was calculated to evaluate recession rate, as this captures the lag associated with infiltration and drainage of water (Braatne et al., 2007; Burke et al., 2009; Kalischuk et al., 2001; Rood & Mahoney, 2000). The daily recession rate (i.e., decrease in WSE) for a given cell is calculated with a 4-day moving window that retains the last three days $\widetilde{WSE}_e$ values ($\widetilde{WSE}_{e,-3}$, $\widetilde{WSE}_{e,-2}$, $\widetilde{WSE}_{e,-1}$, WSE_e). The following equation is used to calculate the 3-day average recession rate (r) for a given day:

$$r = \frac{\widetilde{\mathrm{WSE}}_{e,\,-3} - \widetilde{\mathrm{WSE}}_{e}}{3} \tag{2}$$

The 3-day moving average for the recession rate is calculated as the change in WSE rather than calculating the recession rate for each day. Each day is categorized as a lethal or stressful day by comparing the 3-day average to the recession rate threshold parameters (Table 4), which should be informed by species specific observational or experimental data. The total days tracked during the recruitment period is used to calculate a raster of favorable recession days by subtracting the total lethal and stressful days.

The mortality coefficient (M) was developed to account for seedlings' ability to survive lethal rates of stage decline if the drop in stage is for only a few days (Braatne et al., 2007; Burke et al., 2009). The mortality coefficient is a cumulative metric which considers the percent of days with lethal and stressful recession rates during the desiccation survival period. As this percentage rises, seedlings experience increased stress and mortality from desiccation. The mortality coefficient is defined as:

$$M = \frac{(\%days_{lethal} \times 3) + (\%days_{stress} \times 1)}{3} \quad (3)$$

where $\%days_{lethal}$ and $\%days_{stress}$ are the number of days that the 3-day moving average of the recession rate is considered lethal or stressful, respectively, divided by the total days tracked in the desiccation survival period. Cells with a mortality coefficient below 20 indicate favorable conditions, 20-30 indicate stressful conditions, and above 30 indicate lethal conditions for desiccation survival (Table 5). The mortality coefficient calculation is extremely sensitive to the number of total days that desiccation is tracked, particularly when the number of days between the beginning of seed dispersal and baseflow is short.

A similar dimensionless water stress parameter was used to model desiccation survival of cottonwood seedlings on the Sacramento River (Wang et al., 2018). Both methods calculate the cumulative stress based on the recession rate. Despite the limitations of this metric, the mortality coefficient was selected as it has been successfully used in other similar model applications (Benjankar et al., 2014, 2020; Burke et al., 2009; Tranmer et al., 2023).

To address the sensitivity of the mortality coefficient associated with the total days, the RSRM determines the total days of the desiccation survival period on a cell-by-cell basis starting with the last day a cell goes dry during the seed dispersal period. The desiccation survival period ends at the beginning of baseflow conditions, which is a temporal-recruitment parameter set by the user (Table 3). It is important that the flow record is reviewed and the DOY when baseflow conditions begin is determined as this will influence the total number of days used to calculate the mortality coefficient.

2.9. Prolonged inundation analysis

When $\widetilde{WSE}_e >$ DEM in a cell, inundation is recorded. Inundation tracking counts the consecutive days that inundation is experienced at a cell by overwriting the day count at a given cell with each day that continuous inundation is experienced. At the end of the inundation analysis period, the maximum consecutive inundation days raster (i_{max}) is saved and used to calculate the inundation survival raster by comparing the recruitment threshold parameters (Table 4) for stressful inundation (i_s) and lethal inundation (i_L).

This method assumes that inundation depth is not relevant, a conservative approach. Some studies have found that cottonwood seedlings have a higher tolerance for inundation up to the soil surface and higher mortality for complete shoot submergence due to the decrease in transpiration, inhibition of photosynthesis, and limited oxygen (Amlin & Rood, 2001; Auchincloss et al., 2012; Kozlowski, 2002; Neuman et al., 1996). Future model developments could account for inundation depth with separate threshold parameters for root and shoot depth tolerances.

Table 5
Hydrophysical processes condition and associated metric value.

Hydrophysical process	Condition	Metric value
Bed preparation (bp_{ras})		
$Q_{mobile.f} \leq Q_{max}$	Fully prepared	1.0
$Q_{mobile.p} \leq Q_{max} < Q_{mobile.f}$	Partially prepared	0.5
$Q_{mobile.p} > Q_{max}$	Unprepared	0.0
Desiccation survival (ds_{ras})		
$M_{ras} < 20$	Favorable recession	1.0
$20 \leq M_{ras} \leq 30$	Stressful recession	0.5
$M_{ras} > 30$	Lethal recession	0.0
Inundation survival (is_{ras})		
$i_{max} < i_s$	Favorable inundation	1.0
$i_s \leq i_{max} \leq i_L$	Stressful recession	0.5
$i_{max} > i_L$	Lethal recession	0.0
Scour survival (ss_{ras})		
$Q_{max} < Q_{mobile.p}$	Undisturbed	1.0
$Q_{mobile.p} \leq Q_{max} < Q_{mobile.f}$	Partially disturbed	0.5
$Q_{mobile.f} \leq Q_{max}$	Fully disturbed	0.0

2.10. Hydrophysical process metrics

An initial set of rasters are calculated with input rasters (DEM, depth, WSE, velocity, substrate) and the recruitment parameters that are used to determine the condition that the hydrophysical processes create based on the hydrological regime of the year analyzed. These initial rasters include: (1) partially ($Q_{mobile.f}$) & fully ($Q_{mobile.f}$) mobilized area during the bed preparation period, (2) total days with favorable (d_{fav}), stressful (d_{stress}), & lethal (d_{lethal}) recession rates, (3) maximum consecutive inundation days (i_{max}), and (4) a germination area (A_{germ}).

Each of the hydrophysical processes, except establishment, is assigned a metric criterion indicating condition created in each cell (Table 5). Bed preparation is evaluated by comparing the maximum flow ($Q_{max,b}$) during the bed preparation period to the fully mobilized ($Q_{mobile.f}$) and partially mobilized ($Q_{mobile.p}$) rasters to create the bed preparation raster (bp_{ras}) with metric values that represent the condition of the cell being fully or partially prepared or unprepared. The total days with favorable (d_{fav}), stressful (d_{stress}), and lethal (d_{lethal}) recession rate rasters are used to calculate a mortality coefficient raster (M_{ras}). The mortality coefficient thresholds (Braatne et al., 2007) are used to assign metric values that represent the cell having favorable, stressful, or lethal desiccation survival conditions to create a desiccation survival raster (ds_{ras}). The maximum days of inundation raster (i_{max}) is compared to the inundation threshold parameters to assign metric values that represent the cell having either favorable, stressful, or lethal prolonged inundation conditions. Scour analysis uses the same rasters as the bed preparation analysis and creates a final scour survival raster (ss_{ras}), but the maximum flow ($Q_{max,s}$) is from the scour survival period.

2.11. Combined recruitment potential classes

The combined recruitment potential class for a given cell is calculated as the product of metric values for each of the hydrophysical processes, resulting in a value between 0 and 1, where 1 (optimal class) indicates favorable conditions for all hydrophysical processes and 0 (lethal class) indicates at least one hydrophysical process with lethal conditions (Table 6). Each hydrophysical process with stressful conditions results in a halving of the combined recruitment potential metric. Additional coefficients could be used to weight the relative importance of each hydrophysical process, though by default they are weighted equally at this time. The final outputs from the model include the combined recruitment potential raster and a tabular record of total area of each metric value for all hydrophysical processes and for each combined recruitment potential class. The recruitment potential raster is a map of the suitability of a site for seedling recruitment, which is essentially a lifestage-specific habitat suitability map.

3. Model performance evaluation

For this study, we present the 'implementation verification' of the model with two datasets to demonstrate that the model is free from programming errors and that it performs as described (Augusiak et al., 2014). This approach can ensure that a conceptual model has been implemented into a numerical representation as intended. First, RSRM verification uses a single artificially designed river channel and then

Table 6
Final combined recruitment potential classes.

Recruitment potential class	Stressful processes	Metric value
Optimal	0	1
Favorable	1	0.5
Stressful	2	0.25
Tolerable	3	0.125
Likely Lethal	4	0.0625
Lethal	–	0

applies five different hydrologic regimes to evaluate model behavior. Each hydrologic regime consists of a synthetic record of mean daily discharges for two years that isolates and triggers a single hydrophysical process while holding the rest constant with favorable conditions. The response to each scenario is then traced through the RSRM simulation to determine if the expected recruitment potential outcome is observed. The raster files and flow records required to reproduce this evaluation are provided on GitHub in the River Architect repository. Second, a real site on the lower Yuba River, California, USA is used to illustrate model results where there is complex topography and substrate resulting from dynamic flow and sediment regimes. The site is a geomorphically dynamic, active point bar on which cottonwood seedling recruitment and mortality occur. This site is representative of conditions that can be found in semiarid, gravel-bed rivers worldwide.

3.1. River archetype and model design

A river corridor with laterally connected channel, floodplain, and terrace landforms was synthesized as a simple archetype (Fig. 3). The archetype is meant to mimic topographic features of rivers where cottonwood recruitment is commonly observed but simplified with symmetrical, monotonically increasing lateral slopes. Thus, expected RSRM results can be described precisely with WSEs. Given an ideal annual hydrologic pattern, gentle lateral floodplain slopes allow for gradual stage change. Floodplain connectivity allows for the establishment of seedlings at a high enough elevation to avoid inundation during low flow and scouring flows during the winter following recruitment. The target area defined by the highest and lowest flow during seed dispersal, or the germination area, on the floodplain (0.75-1.25 m above baseflow) will remain constant throughout all scenarios.

The uniform, straight trapezoidal channel has bottom and top widths of 10 and 20 m with a maximum depth of 0.5 m, implying a bank gradient of 10:1. The channel and valley floor have a 0.1 % slope. The floodplain width at double that depth is 120 m, so the entrenchment ratio is 6.0 implying the channel is not entrenched but is instead well connected to the floodplain. In turn, the floodplain has a lateral slope of 1 % going from 110 to 220 m wide from the bank tops to the terrace toes. Flat terraces span the rest of the valley, which is 420 m wide. The DEM created from this geometry and all input rasters are 1 m x 1 m grids.

This study used TUFLOW HPC (v. 2023-03-AE) for 2D hydrodynamic modeling (BMT-WBM, 2018). The discharges simulated were 1.06 (filling half the height of bankfull), 3.89 (bankfull), 25.40 (filling half the height of the floodplain), 53.64 (filling three-quarters the height of the floodplain), 98.75 (floodplain-filling), 111.06 (0.05 m inundating terraces), 178.22 (0.25 m inundating terraces), and 293.00 m^3/s to span the low flow to valley wide flood conditions (Fig. 3). Because the terrain and flow regime are artificial, validation is not possible for this exploratory modeling evaluation. In any case, 2D models have

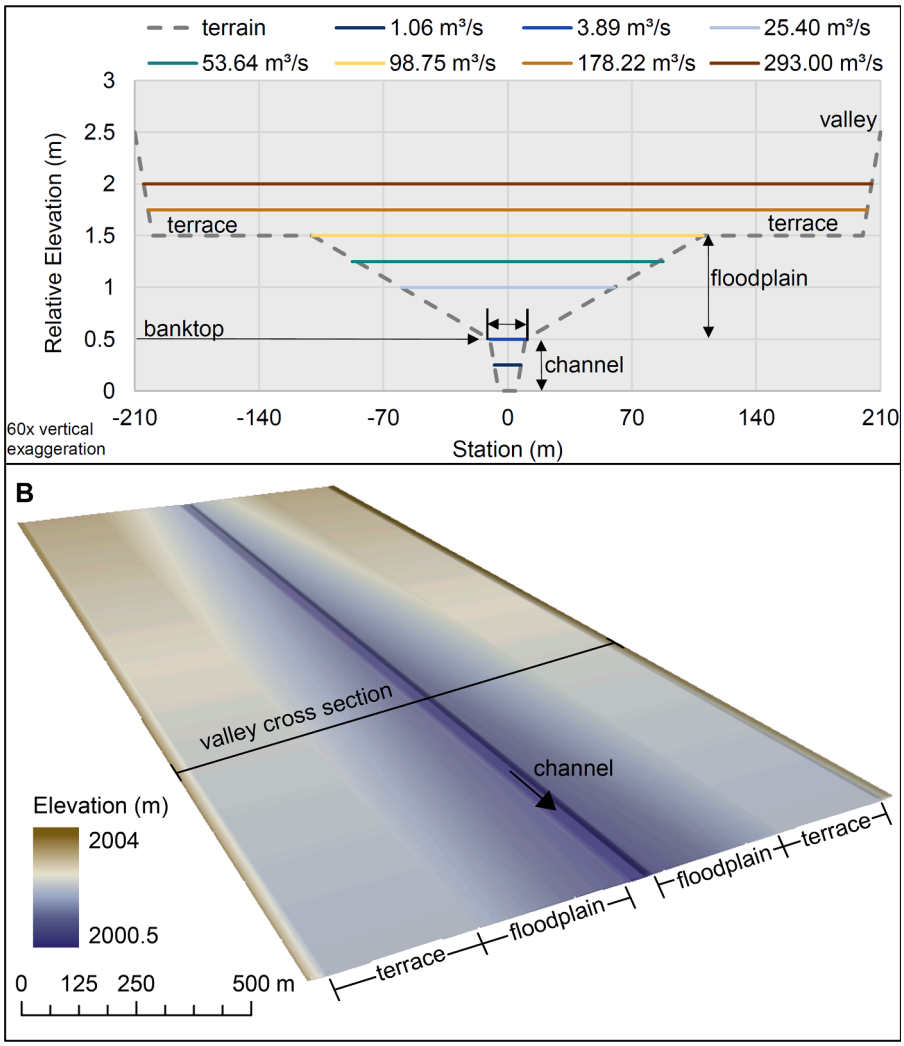

Fig. 3. Cross-sectional view of the terrain (A) developed to test the RSRM model with water surface elevations for the 2D modeled discharges. Note that 60x vertical exaggeration is used to make the lateral features easy to view. The 3D view of the DEM (B) shows the terrain without exaggeration to illustrate the gentle slopes of the wide floodplain relative to the channel.

outstanding performance in such simple cases.

3.1.1. Hydrologic scenarios

Five characteristic hydrologic scenarios spanning a single recruitment potential assessment period were simulated for the river archetype (Fig. 4). An idealized hydrograph with optimal recruitment conditions over a sizable germination area was developed as the first scenario to be evaluated to confirm the understanding of perfect recruitment and ensure that the model achieved that expectation. This idealized hydrograph contains the required hydrologic features necessary to create optimal conditions for seedling recruitment across the floodplain (0.75-1.25 m above baseflow).

Scenarios 1, 2, 4, and 5 have a baseflow start date of September 15th. Scenario 1 begins with a peak flood event (293.00 m^3/s) that prepares the bed for germination the winter before seed dispersal. This flood event is large enough to fully mobilize the sediment across the entire germination area. This area was targeted for the germination area as it is fully mobilized by the valley-filling flood events and on a gradual slope that allows for different recession rate scenarios to be tested within the same germination area. The stage recedes slowly through most of the seed dispersal period and to baseflow conditions (1.06 m^3/s) beginning on September 15th, which should create favorable recession conditions. The stage does not rise again above the lowest flow during seed dispersal (0.75 m above baseflow), so prolonged inundation stress and scour should not affect the germination area.

The remaining four scenarios use the idealized hydrograph in Scenario 1 (ideal conditions) each with a single experimental manipulation to change the outcome of recruitment potential with respect to a single recruitment metric (Fig. 4). Scenario 2 (decreased prepared germination sites) evaluates the behavior of the bed preparation threshold parameters by changing the peak flood event from 293.00 to 98.75 m^3/s. Scenario 3 (increased desiccation stress and mortality) evaluates the behavior of the recession rate parameters by increasing recession rate after the seed dispersal period and changing the start of baseflow. Scenario 3 is the only scenario for which discharge drops rapidly in early summer to baseflow (1.06 m^3/s), so the baseflow start date for Scenario 3 is July 1st. Scenario 4 (increased inundation stress and mortality) evaluates the behavior of the prolonged inundation threshold parameters by including a 14 day period in the winter after recruitment where discharge rises to 53.64 m^3/s, inundating the lower half of the germination area. Scenario 5 (increased scour stress and mortality) evaluates the behavior of the scour threshold parameters by including a winter flood (98.75 m^3/s) in February after recruitment. The following subsection describes how the expectations were developed that model results were vetted against.

3.1.2. Scenario expectations

Model evaluation involves transparently stating the expectations of the spatial pattern and metric values for cottonwood recruitment potential for each hydrologic scenario based on the conceptual model and then determining if model results matched expectations. Model results for all scenarios were analyzed by comparing the expected elevation bands and total area breakdown of recruitment potential classes and number of days of favorable, stressful, and lethal recession to the observed results. Expected elevations (above baseflow) for the breaks of metric values were determined from τ_* rasters for Scenarios 2 and 5 and from the elevations calculated based on the depth of water of the modeled flows for the germination area and Scenario 3 (Fig. 3).

Elevations of the desiccation survival bands are complex to predict without the $\widetilde{WSE}_e$ produced by the RSRM, as the total days tracked is variable throughout the germination area and that total significantly influences the mortality coefficient calculation. Rather than calculate expected elevations bands, the number of favorable, stressful, and lethal days expected were determined from daily flows by linearly interpolating between the WSEs of modeled flows (see Fig. 3) and then calculating the 3-day average recession rate. The expectations for favorable, stressful, and lethal days are summarized in Table 7.

The expected elevation of the bands for the conditions and corresponding metric value are summarized in Table 8 for Scenarios 1, 2, 4, and 5. The expected total area for each metric value for all scenarios was

Table 7
Expectations for total number of favorable, stressful, and lethal recession days.

Hydrologic feature	Rate	Recession periods	Expected results
Scenario 1:			
Stage slowly recedes (≤ 2.5 cm/day) after seed dispersal ends until baseflow conditions reached (Sept. 15th)	$r_s > r$	Tracking begins between May 3rd (1.25 m above baseflow) to June 20th (0.75 m above baseflow) Tracking ends Sept. 15th	88 - 136 days
	$r_s \leq r < r_L$	None	0 days
	$r \geq r_L$	None	0 days
Scenario 3:			
Stage quickly recedes (>2.5 cm/day) after seed dispersal ends until baseflow conditions reached (July 1st)	$r_s > r$	Tracking begins between May 3rd (1.25 m above baseflow) to June 20th (0.75 m above baseflow) Last favorable day June 20th	1 - 49 days
	$r_s \leq r < r_L$	June 21st - 22nd	2 day
	$r \geq r_L$	June 23rd - July 1st	9 days

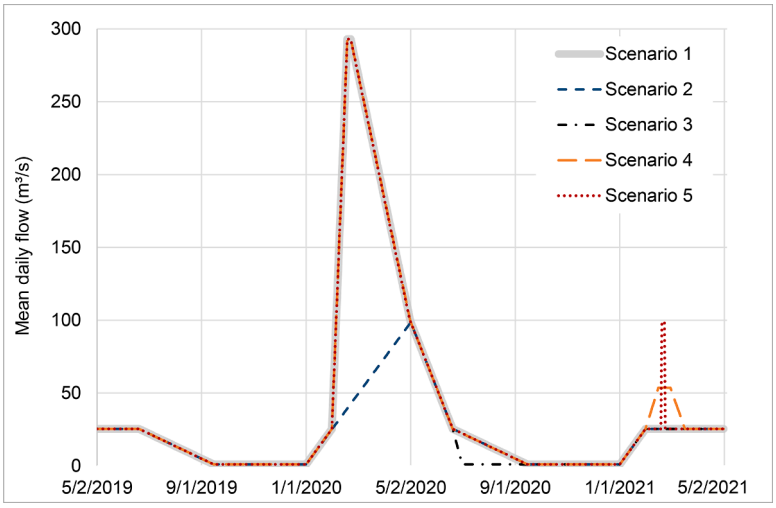

Fig. 4. Hydrographs of the five scenarios used to evaluate the RSRM implementation.

Table 8
The expected elevation bands from Scenarios 1, 2, 4, and 5 with the corresponding condition satisfied by the hydrologic feature driving the process and metric value.

Hydrologic feature	Elevation above baseflow	Condition satisfied	Metric value
Scenario 1: Ideal conditions	0.75 – 1.25	$\tau_* \geq 0.047$ $r < 2.5$ cm/day $i_{max} < 14$ days $\tau_* < 0.030$	1.0
Scenario 2: Decreased prepared germination sites	1.00 - 1.25 m	$\tau_* < 0.030$	0.0
	0.86 – 1.00 m	$0.030 \leq \tau_* < 0.047$	0.5
	0.75 – 0.86 m	$\tau_* \geq 0.047$	1.0
Scenario 4: Increased inundation stress and mortality	1.00 - 1.25 m	$i_{max} < 14$ days	1.0
	0.87 – 1.00 m	14 days $\leq i_{max} \leq$ 28 days	0.5
	0.75 – 0.87 m	$i_{max} >$ 28 days	0.0
Scenario 5: Increased scour stress and mortality	1.00 - 1.25 m	$\tau_* < 0.030$	1.0
	0.86 – 1.00 m	$0.030 \leq \tau_* < 0.047$	0.5
	0.75 – 0.86 m	$\tau_* \geq 0.047$	0.0

calculated from the width of the bands given the constant slope and height from the elevations and the length of the reach evaluated (250 m). The area of the vegetation patches for each band are subtracted to account for the removal of these areas from the analysis. The germination area for all scenarios is expected to be between 1.25 m above baseflow and 0.75 m above baseflow, which are the highest and lowest stages during seed dispersal. The total area that falls between 0.75-1.25 m above baseflow for the 250 m long river archetype calculated geometrically is 25,000 m^2. There should be no recruitment prediction outside of the germination area and existing vegetation should be removed from the left bank analysis area where the vegetation raster delineates presence (25 squares; 1,000 m^2 total) resulting in a total recruitment potential area of 24,000 m^2. The Supplementary Materials contains detailed descriptions for each scenario expectation.

3.2. Real-world example: lower Yuba River

The study uses a site on the lower Yuba River (LYR) – a dynamic, regulated river in a semiarid climate in north central California, USA – to demonstrate the simulation of the potential seedling recruitment niche

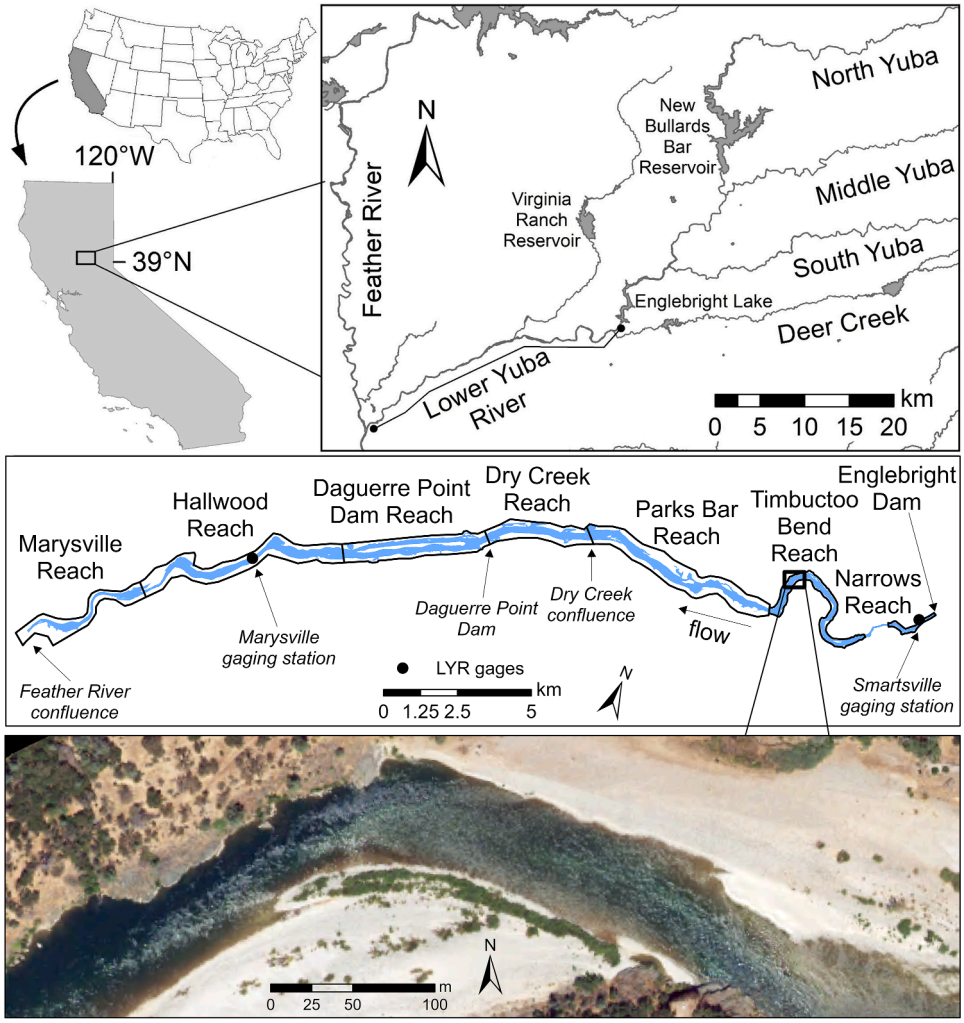

Fig. 5. Location of the lower Yuba River and the eight geomorphic reaches, including the key reach break landmarks and USGS gaging stations.

with complex hydrology and topography. The 37.1-km LYR segment drains ~ 3,480 km^2 of the western Sierra Nevada foothills flowing east to west from Englebright Dam to the Feather River (Fig. 5). The LYR is a regulated single-thread gravel-cobble bed channel with a high width-to-depth ratio that is meandering to straight in pattern (Wyrick & Pasternack, 2014).

The dominant vegetation in the floodplain of the LYR includes Fremont cottonwoods (*Populus fremontii*), willows, and box elder with an understory of elderberry or Himalayan blackberry shrubs (USACE, 2012, 2014). *Populus fremontii* (*P. fremontii*) is one of the most important riparian species in California as it is a historically dominant species of riparian forests in the Central Valley as well as across the southwestern USA and northern Mexico (Conard et al., 1977; Hultine et al., 2020). The pre-settlement Sacramento River forest, spanning from below Sacramento to above Red Bluff, extended an estimated 206,000 hectares and today the riparian forests of the entire Central Valley span approximately 41,300 hectares (Katibah, 1984).

A study site was selected downstream of Englebright Dam in the Timbuctoo Bend Reach (TBR). The TBR begins downstream of a steep-walled bedrock canyon that widens into a bedrock valley with some meandering characterized by active gravel bars, non-uniform channel geometry, and a well-connected floodplain (Sawyer et al., 2010). The site of interest selected for this example is a point bar with a vegetated swale that is well connected to the floodplain.

Streamflow data for the 2017 recruitment year for the Timbuctoo Bend reach is the combined flow from U.S. Geological Survey (USGS) Smartsville gage (#11418000) and Deer Creek gage (#11418500). A total of 43 flows from 11.33 to 2389.94 m^3/s were used to model the range of discharges that occurred during the 2017 recruitment year period (Fig. 6). The parameter (temporal and threshold) values used for simulating the TBR site with the RSRM are based on expert-opinion; they were not calibrated (Table 9).

The RSRM requires topographic, hydraulic, sediment size, and vegetation presence raster data (Fig. 7). Topographic data for the study site is from a 0.91-m-resolution 2017 topo-bathymetric DEM. Source data were collected using near-infrared and green airborne LiDAR, boat-based multi-beam echosounding, and ground-based RTK GPS surveys (Silva & Pasternack, 2018). Airborne LiDAR data was also used to map 2017 vegetation, yielding an established-vegetation presence/absence (defined as taller than 0.6 m) raster and a canopy height raster. TUFLOW HPC (v. 2023-03-AE) for steady-state, 2D hydrodynamic modeling was used to model 2017 LYR velocity, depth and WSE at 1-m resolution for the whole river segment (Pasternack, 2023). A 2017 LYR subaerial sediment grain size raster was available from a previous study that measured grain size distributions for the 2017 LYR sediment facies and then used that training data in a random forest machine learning model, along with 15 topo-bathymetric variable rasters, to predict the spatial pattern of sediment facies map with an 86 % 10-fold cross-validation accuracy (Díaz Gómez et al., 2022).

Table 9
Recruitment parameters (temporal and thresholds) used for the TBR site.

Parameter	Value	Reference
1. Seed dispersal period		
Start day	May 2nd	Species and site specific decision.
End day	July 4th	
2. Bed preparation period	2 year	Site specific decision
3. Critical dimensionless bed shear stresses		
Fully prepared	$\tau_{*f} = 0.047$	Lamb et al., 2008; Shields, 1936
Partially prepared	$\tau_{*p} = 0.030$	
4. Baseflow period start		
Start day	September 15th	Determined from daily flow record.
5. Recession rate (cm/day)		
Stressful rate	r_s =1 cm/day	Amlin & Rood, 2002; Mahoney & Rood, 1998; Stella & Battles, 2010
Lethal rate	r_L = 2.5 cm/day	
6. Prolonged inundation (days)		
Stressful inundation	i_s = 14 days	Auchincloss et al., 2012
Lethal inundation	i_L= 28 days	

4. Results

4.1. Canonical test channel

All scenarios produced recruitment potential predictions only within the conceptualized germination area. All germination area, hydrophysical process, and combined recruitment potential rasters for all scenarios were reviewed and have the expected 1,000 m^2 of vegetated area that falls within the germination area removed. The total recruitment potential area and germination area for all scenarios was 23,750 m^2 compared to the expected 24,000 m^2, producing a negligible 1 % (250 m^2) difference (Table 10). Vertical differences between the expected and observed upper and lower boundaries of the germination area were negligible 7 and 2 mm, respectively (Table 11). The observed

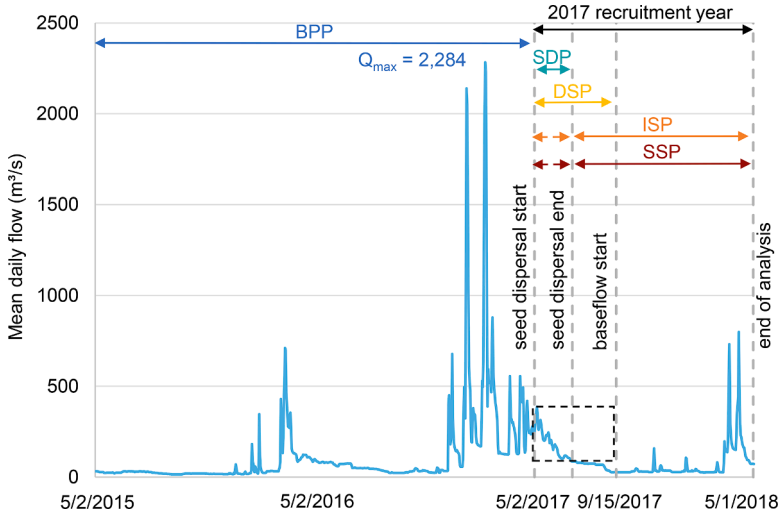

Fig. 6. Hydrograph of the combined flow measured at the USGS Smartsville gage (#11418000) and Deer Creek gage (#11418500) with the recruitment box and temporal analysis periods.

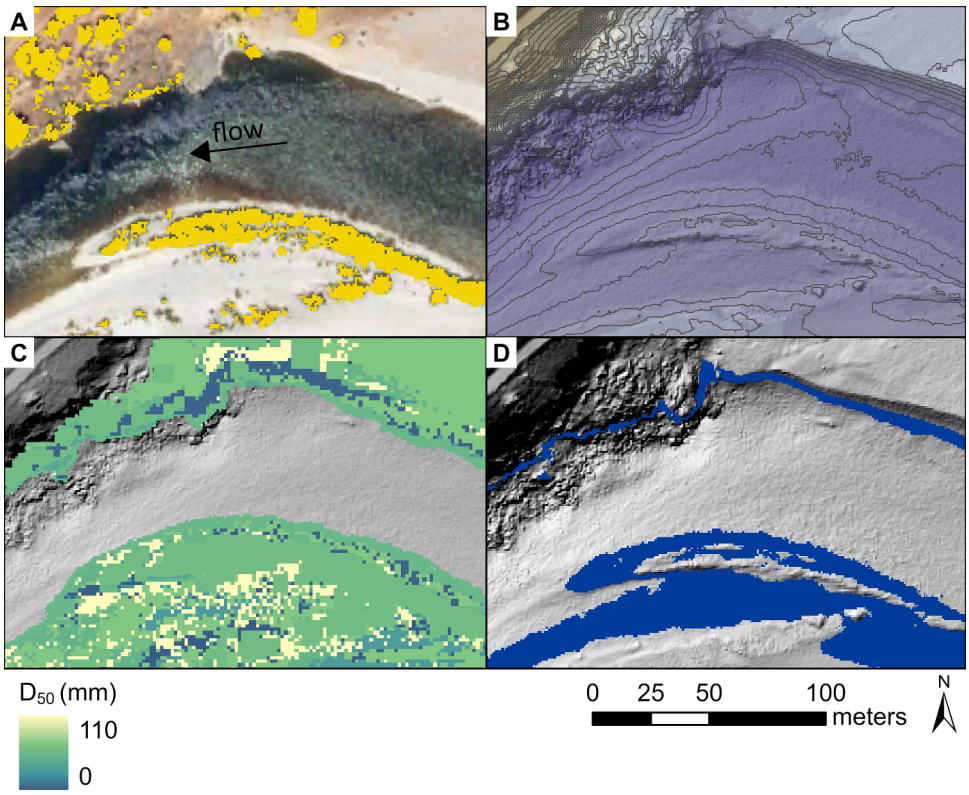

Fig. 7. Study site rasters showing (A) plan-view aerial imagery with vegetation overlay (yellow), (B) DEM (darker blue is lower elevation), (C) grain size, and (D) hillshade with wetted area overlay (blue).

Table 10
Total difference in area (m^2) between the expected and observed combined recruitment potential areas for the five scenarios. Expected total area is 24,000 m^2 and the observed total area is 23,750 m^2 for all scenarios.

Scenario	Optimal (1.0)	Favorable (0.5)	Lethal (0.0)	Total Area
1	250	0	0	250
2	250	0	0	250
3*	–	–	–	250
4	250	0	0	250
5	0	0	250	250

*No total difference in area for the combined recruitment potential classes for Scenario 3 as expected areas were not calculated (see 3.1.2 Scenario expectations).

total favorable, stressful, and lethal recession rate days met the expected days exactly for Scenario 1 and 3 (Table 7). The RSRM model outputs were also laterally symmetric and longitudinally constant because the applied river channel geometry is laterally symmetric with a constant slope (Fig. 8). The full set of input and output rasters are presented in the Supplementary Materials. This allows for a simplified 1D cross-sectional visualization of all model results (Fig. 9). The corresponding break lines for each metric value are shown in Table 11.

For Scenario 1, conditions were optimally favorable for bed preparation as well as survival of desiccation, inundation, and scour/burial, resulting in optimal total recruitment potential along the recruitment band determined by the range of wetted areas during seed dispersal. The limited bed preparation flow from Scenario 2 resulted in bands of unprepared bed at the highest elevations (where shear stresses were minimal), fully prepared bed at the lowest elevations (where shear stresses were greatest), and a band of intermediate partially prepared bed. Because all other hydrograph features were unchanged and provided optimal recruitment potential for the corresponding hydrophysical processes, the total recruitment potential was identical to the bed preparation raster, indicating that bed preparation served as the limiting process in this scenario (Fig. 9).

Table 11
Expected versus observed elevations (above baseflow) for the breaks between metric values and the vertical difference between expected and observed elevations for the five hydrologic scenarios. All scenarios have the same elevations for the upper and lower boundary of the germination area.

Scenario	Elevation band boundary	Expected elevations (m)	Observed elevations (m)	Difference (m)
All	Upper	1.250	1.243	0.007
	Lower	0.750	0.748	0.002
2	Metric value 0 to 0.5	1.000	1.000	0.000
	Metric value 0.5 to 1	0.860	0.860	0.000
4	Metric value 0.5 to 1	1.000	0.998	0.002
	Metric value 0 to 0.5	0.865	0.868	−0.002
5	Metric value 0.5 to 1	1.000	1.000	0.000
	Metric value 0 to 0.5	0.860	0.860	0.000

The Scenario 3 hydrograph's more rapid stage decline during the period between germination and baseflow resulted in a range of mortality coefficients and corresponding recruitment potential metrics. The uppermost band goes dry before the more rapid stage decline, resulting in a higher proportion of days between going dry and reaching baseflow. The percent days of lethal and stressful recession decreases as the total days of the desiccation survival period increases resulting in a lower mortality coefficient (i.e., favorable recession/desiccation survival conditions). Meanwhile, lower bands remain inundated for longer resulting in fewer total recession days tracked, which begins when the cell dries. The result is a higher mortality coefficient as the total days of

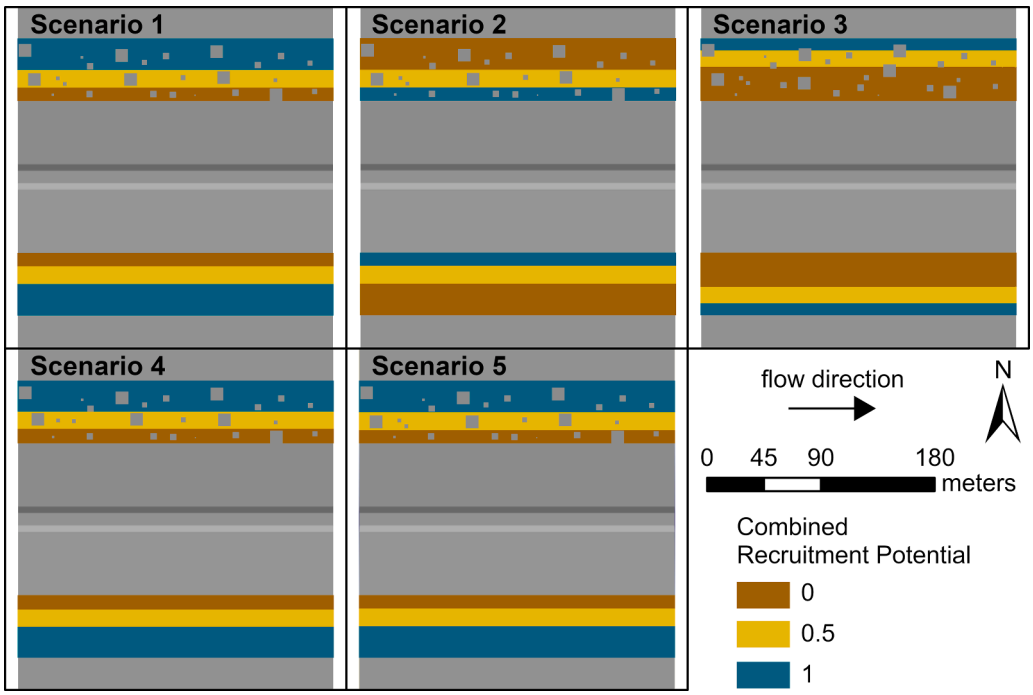

Fig. 8. Plan-view of the combined recruitment potential rasters for each scenario. Vegetation rasters only had vegetation on the left bank (i.e., blank squares in the top area of each map).

the desiccation survival period decrease, increasing the percent days of lethal and stressful recession. All cells in the germination area experience 2 stressful days of recession and 9 lethal days of recession as expected (Table 7), so the mortality coefficient changes based on the total days tracked. This resulted in bands of stressful and lethal desiccation survival at lower elevations (Fig. 9).

The Scenario 4 hydrograph's gradual rise in stage after reaching baseflow and prolonged inundation before ramping back down led to inundation stress and mortality. Because the maximum stage during this period is 1.0 m above baseflow, the band above this stage maintained optimally favorable inundation survival conditions, while the lowermost band was inundated for 29 days resulting in lethal conditions. An intermediate band corresponds to regions that were inundated for a shorter time period corresponding to stressful conditions (Fig. 9). Inundation was the only non-optimal hydrophysical process for this condition and thus limited total recruitment.

Finally, Scenario 5 had the same peak flood as Scenario 2, but because it occurred following seed dispersal and germination rather than before, it had the effect of limiting recruitment potential via scouring of seedlings rather than preparing the bed as in Scenario 2. Due to the corresponding maximum shear stresses during the scour period of Scenario 5 being identical to those during the bed preparation period of Scenario 2, the bands of optimal scour survival in Scenario 5 correspond to unprepared bed in Scenario 2, while the bands of lethal scour in Scenario 5 correspond to bands of optimal bed preparation in Scenario 2. The intermediate band also matches corresponding to partially prepared bed in Scenario 2 and partial scour in Scenario 5 (Fig. 9).

4.2. Timbuctoo Bend site

The area of seedling recruitment potential is limited to the wetted area during seed dispersal (potential germination area), defined by the smallest and largest flows during this period (Fig. 7). Areas with established vegetation defined by the input vegetation raster are removed from this wetted area where germination is possible. Areas that are fully prepared (1.0) are primarily concentrated near the main channel corresponding with the areas in the fully mobilized flow raster with flows that are smaller than the peak winter flood event (2283.60 m^3/s) during the bed preparation period (Fig. 10). The largest area that is partially prepared (0.5) occurs in the vegetated swale corresponding with the areas in the partially mobilized flow raster that are mobilized by the peak winter flood and lesser flows. The remaining area within the potential recruitment area is unprepared (0). Conversely, most of the potential area is undisturbed (0) by flows after seedlings are established. A patchy strip along the upstream side of the point bar has fully disturbed (0) and partially disturbed (0.5) area.

Favorable recession (1.0) and lethal inundation (0) areas are present in bands along inner boundary of the recruitment potential area and vegetated swale (Fig. 11). The remaining area experiences stressful recession (0.5) with no lethal recession (0) conditions. A majority of the remaining recruitment potential area has favorable inundation (1.0) conditions with a thin row of stressful inundation (0.5) between the favorable and lethal areas and a patch in the vegetated swale. The combined recruitment potential raster is predominately lethal (0) with optimal (1.0), and favorable (0.5) potential recruitment sites found in the vegetated swale and a band on the point bar (Fig. 12).

5. Discussion

The objective of this study was to develop a model that predicts the spatial distribution of potential recruitment sites for riparian seedlings using environmental data. A mechanistic potential recruitment niche model was developed using data and hydraulic modeling products commonly available in river science, including flow records, topo-bathymetry, 2D hydraulic modeling outputs, and substrate data. The functionality of the model was then demonstrated by testing it on a simplified channel with five hydrologic scenarios and presenting an example of the results for a real river.

5.1. Canonical test channel evaluation

The discrepancy between expected and observed total areas can be explained by the vertical difference between expected and observed elevations of the germination area boundaries. This vertical shift in the

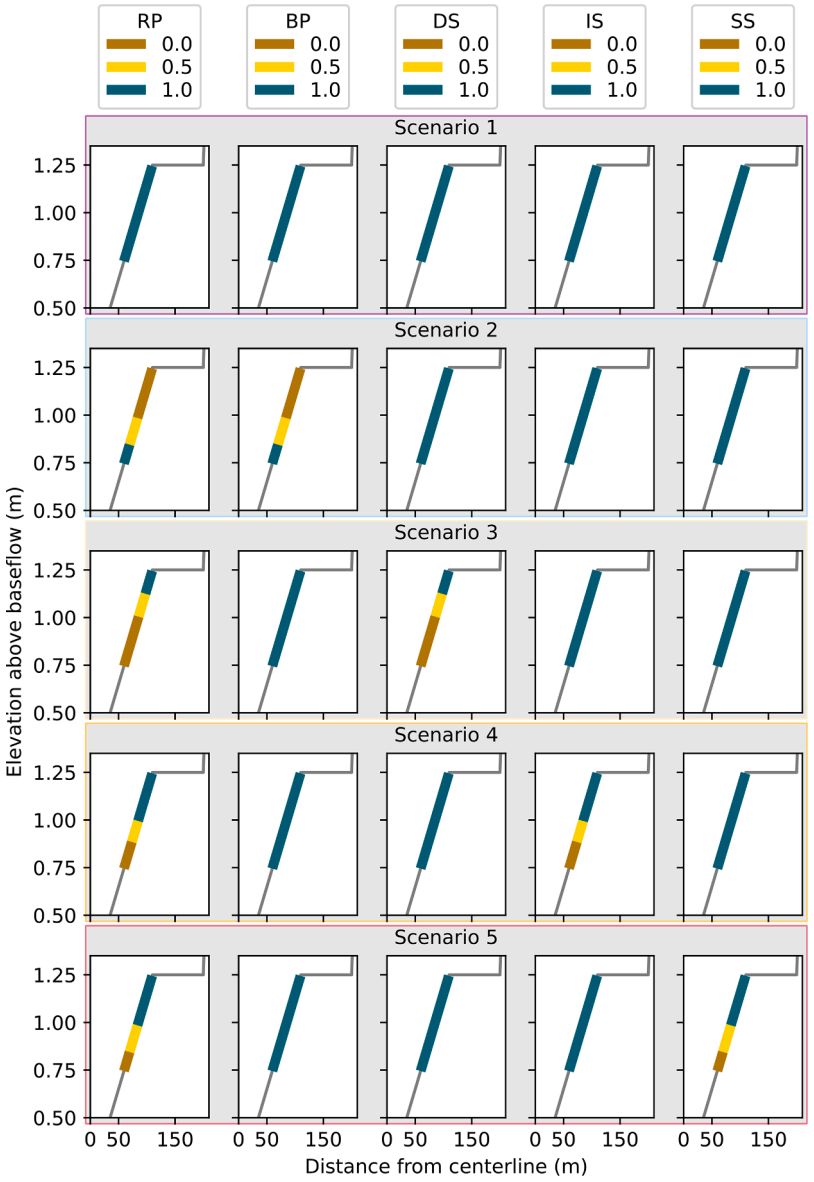

Fig. 9. Cross-sectional view of RSRM rasters (RP = combined recruitment potential, BP = bed preparation, DS = desiccation survival, IS = inundation survival, SS = scour survival) for each evaluation scenario. The change in the hydrologic feature for each scenario (no peak winter flood, increased recession rate, prolonged inundation event) triggers stressful and lethal conditions for the hydrophysical process associated with the feature that results in the change in the overall combined recruitment potential.

germination area results in a 5 mm total vertical difference, which corresponds to the vertical difference of a single cell (0.5 m wide) on the 0.1 % floodplain side slope. The total width of the germination area is expected to be 50 m, while the observed width is 49.5 m, with the difference being equivalent to a single row of cells (0.5 m wide). The shift is observed on both banks, resulting in an observed area that is 250 m^2 (0.5 m x 250 m long x 2 banks) less than the expected area.

The origin of these discrepancies can be traced to the interpolation of WSE rasters, highlighting the importance of understanding the effects that 2D hydrodynamic models may introduce. With TUFLOW HPC, the default setting for the wet/drying algorithm (which determines the depth at which a wetted cell is set to dry between timesteps) is 2 mm, resetting cells to dry if they fall below this depth (BMT-WBM, 2018). This forces these shallow cells at the edge of the model's wetted area to be dry in the hydrodynamic model outputs, while producing depths of 2 mm when the WSE is extended across the model DEM. This error is apparent in the simplified example used for testing here, but for a complex, real-world terrain, it would be nearly indiscernible. This is the only source of error identified by the evaluation, which demonstrates that the model is functioning as expected. Additionally, the canonical test channel and hydrologic scenario datasets can be used to benchmark other mechanistic riparian seedling recruitment models.

5.2. *Model evaluation methods*

Model evaluation is a multi-step, iterative process. New models are often tested against simple analytical cases or easily interpretable scenarios to confirm that model outputs are consistent with the underlying theory. This method investigates whether the models yield results that align with the well-established conceptual understanding of the dynamics of the phenomenon in question (Fitz et al., 1996; Tucker et al., 2001). The use of a uniform terrain archetype and simplified hydrology allows for quantitative, testable expectations to be applied when evaluating the model, making it well-suited for verifying that the model faithfully represents the underlying processes. It also allows for a new model to be evaluated when empirical data from a real-world system are

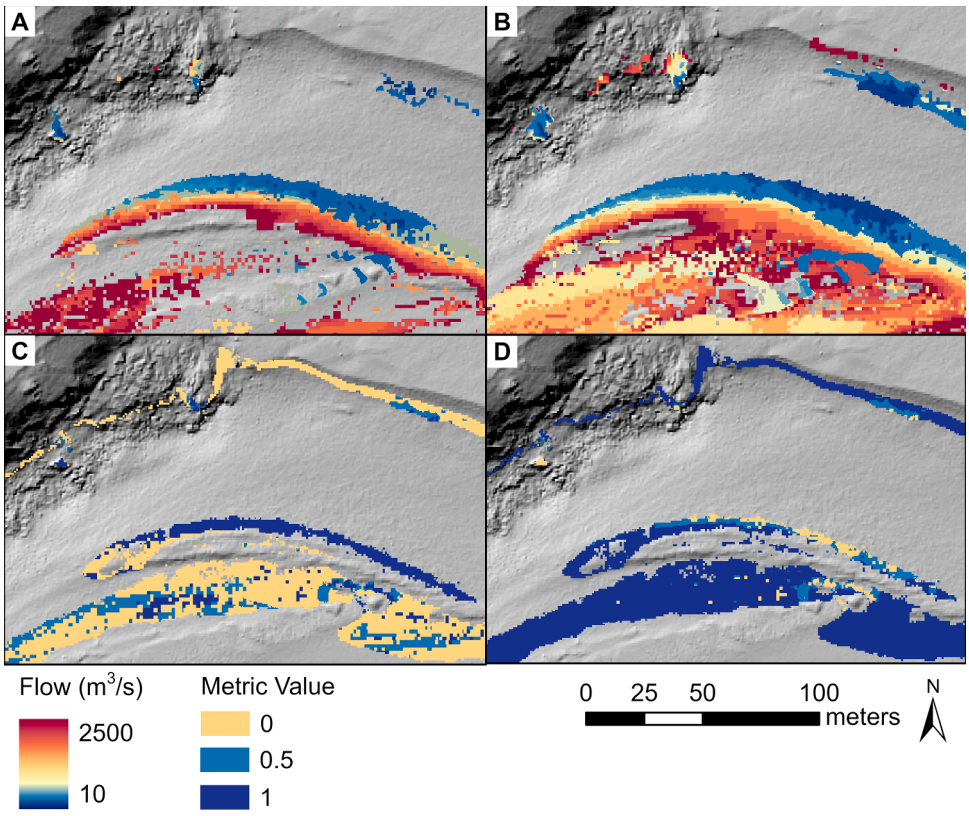

Fig. 10. Bed preparation assessment at TBR site including the (A) fully and (B) partially mobilized flow rasters and the final (C) bed preparation and (D) scour survival rasters.

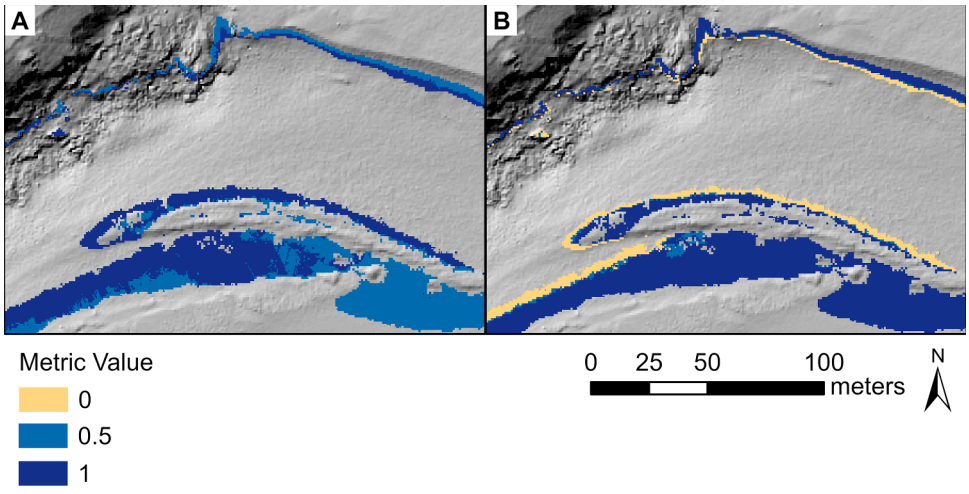

Fig. 11. Final (A) desiccation survival and (B) inundation survival rasters at TBR site.

not available, which is the case in this study.

Synthetic data is limited in its utility because empirical validation data, such as the observed presence or absence of seedlings, do not exist. A real-world site where these observations can be collected is needed for the purposes of calibration and validation. However, real-world sites also introduce a host of complexities that can make attributing model performance issues to specific causal factors highly uncertain. While it is common for a new model to be tested by comparing model outputs with empirical data to 'validate' the model, relying solely on the agreement between model outputs and empirical data can lead to a false sense of accuracy if the model has incorrect or overfit parameterizations or structure, limiting broader applicability (Oreskes & Belitz, 2001).

The hydrophysical processes and combined recruitment potential maps at the TBR site exhibit predictable patterns based on known relationships between topography, hydraulics, and recruitment. For example, lower velocity flows are required to mobilize the bed along the point bar due to deeper, faster-moving flow and moderately sized sediment (Fig. 10). Likewise, lethal inundation is expected to occur at lower elevations near the main channel (Fig. 11). Qualitative expectations of where we will see fully prepared beds or lethal inundation are reasonable, but setting testable elevations or areas for comparison with theory is not possible without completing the geospatial calculations that the RSRM algorithm and 2D hydrodynamic model resolve. A balanced approach acknowledges that both synthetic and real datasets

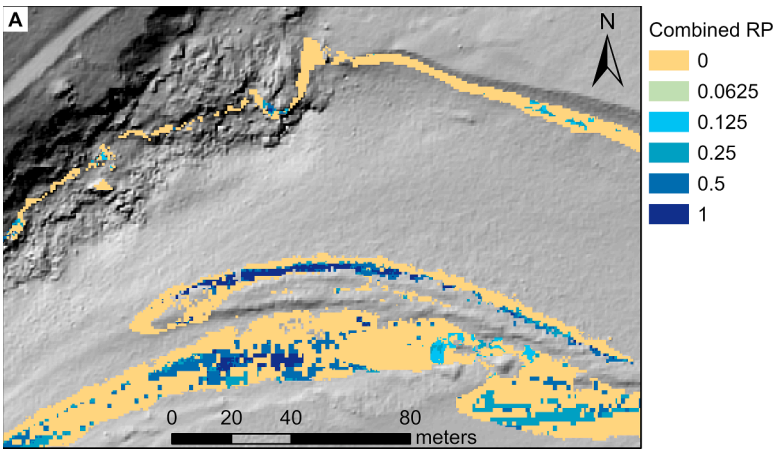

Fig. 12. Combined recruitment potential at the TBR site.

enhance model evaluation, helping to ensure the code functions as intended and aligns with theoretical expectations.

5.3. Comparative model review

Peer-reviewed applications of the recruitment box model have previously analyzed seedling recruitment of cottonwood and other riparian tree and shrub species. Examples include assessing the impacts of dam operations on recruitment (Burke et al., 2009), developing instream flow recommendations to promote recruitment (Rood et al., 2003; Rood & Mahoney, 2000; Stella et al., 2010), and simulating distributions of natural recruitment patterns (Benjankar et al., 2014, 2020; Dixon & Turner, 2006; Tranmer et al., 2023). Models have been developed to analyze the impacts of altered flow regimes on cottonwood seedling recruitment using topographic cross-sections and transect data (Braatne et al., 2007; Burke et al., 2009; Wang et al., 2018). These one-dimensional (1D) approaches require linear interpolation to estimate recruitment potential between cross-sections. Although their methods do not consider physical processes in plan-view 2D space, such as scour and erosion, they do consider the timing and magnitude of peak flows that drive these processes. They also provide a methodology for analyzing recruitment with limited computational demand and input data.

Benjankar et al. (2014) improved on 1D models by considering the same processes with a spatially distributed method and modeling the preparation of suitable germination sites using a mechanistic approach. The Spatially Distributed Cottonwood Recruitment (SDCR) model uses a fuzzy logic approach that creates a set of rules to determine the favorability of recruitment sites (5 m x 5 m cells) for cottonwood seedlings using water surface elevations (WSE) modeled with a 1D hydrodynamic model to calculate local shear stress, stage recession rates, and total inundation duration (Benjankar et al., 2014). A further summary of these previous models and the effects of flow on riparian vegetation dynamics can be found in a comprehensive review by Vesipa et al. (2017).

The SDCR was adapted to analyze riparian seedling recruitment (*Populus* spp. and *Salix* spp.) and restoration alternatives with an improved approach using WSE and velocity results from a plan-view 2D hydraulic model, but it no longer included a winter flood parameter to simulate stress caused by prolonged inundation in a mechanistic manner. The model, therefore, yields an overprediction of favorable recruitment sites in areas that would experience prolonged inundation (Benjankar et al., 2020). Subsequently, the recruitment model of Benjankar et al. (2020) was reconfigured to assess the failing recruitment mechanisms (seed dispersal timing, hydrochory, bed preparation, root growth, and desiccation mortality) over floodplains of varying sizes (Tranmer et al., 2023).

The development of the RSRM advances the pre-existing models in five significant ways. First, existing models do not account for seedling survival during peak flows following the establishment period of interest with a spatially explicit and mechanistic approach. The new model accounts for the processes by which seedling mortality is often dominated by flow pulses that erode or bury new germinants (Dixon, 2003; Johnson, 2000; Kui & Stella, 2016). Second, it defines a germination area (or recruitment band) in a mechanistic way that does not require previous seedling observation data. Third, it accounts for the limitations that existing forest canopy shade imposes on potential germination sites. Fourth, the new model is designed from scratch to be used not only for river assessment but also for river design assessment and improvement before a project has been built. For example, it allows users to specify unique attributes for artificially graded terrain as part of spatially distributed sediment characteristics inputs. Finally, to our knowledge, no other seedling recruitment model that utilizes 2D hydrodynamic model products has been developed and shared with the public as an extensible open-source tool, backed by thorough documentation and a tested dataset that can be used for benchmark testing.

5.4. Future applications and improvements

Predictive models are powerful tools that can aid scientific progress by testing theories in real-world applications and inform river management through evaluating changes in seedling establishment under alternative streamflow management policies, habitat restoration designs, and climate change scenarios. Results from the mechanistic model can also be used to train correlative models to improve predictive accuracy (Horemans et al., 2024). The interaction of biological and physical processes that drive riparian seedling recruitment makes creating a process-based model that mimics the real world a challenging task. There will always be room for improvement when it comes to model development, but this does not mean that a model is not useful given that the associated assumptions and limitations are considered.

For the RSRM, a mechanistic approach that incorporates the life history and physiology of riparian tree seedling recruitment was chosen over a statistical approach. A limitation of statistical approaches, such as presence-absence models, is their inability to determine the relative importance of mechanistic pathways (Caradima et al., 2021). For example, there are strong correlative relationships between successful recruitment bands and topography, such as the height above baseflow (Mahoney & Rood, 1998). The process-explicit approach of the RSRM makes it possible to understand the relative contribution that each hydrophysical process has on recruitment potential beyond correlative relationships. This approach casually links the mechanisms driving a species recruitment responses to environmental processes. However, the reliability gained from the improved structural realism depends on

adequate parameterization to minimize projection uncertainty (Singer et al., 2016).

Preliminary evaluation of the model using a canonical example has demonstrated its basic functionality and reliability. While these initial tests indicate that the model produces expected results under simple conditions, further evaluation and validation are necessary to ensure accurate results with complex, real-world data. Methods for collecting observational data to calibrate and assess model performance in past studies include delineating patch boundaries on aerial photographs (Benjankar et al., 2014) or with RTK GPS (Benjankar et al., 2020) and surveying seedling densities and over-winter mortality rates (Dixon & Turner, 2006). Although observational data enable model calibration to improve accuracy, it is essential to minimize parameter uncertainty when applying a mechanistic model to explore underlying processes. Otherwise, a correlative modeling approach may be a better choice, as it does not require the detailed parameter estimates needed to calibrate mechanistic models (Peterson et al., 2015). Future work should focus on further model evaluation steps, including structural and parameter sensitivity analysis, calibration, and validation with independent data (Augusiak et al., 2014). Potential model improvements could include more accurate modeling of the riparian water table to account for capillarity, geology, and groundwater dynamics, as well as alternative methods for tracking root depth estimates. Further discussion of the model limitations can be found in the Supplementary Materials.

6. Conclusion

Riparian forests continue to suffer from land use change, flow alteration, and climate change, so the need for predictive tools to support management decisions remains a top priority. The RSRM can inform river management by evaluating changes in seedling establishment under alternative streamflow management policies, habitat restoration designs, and characterization of baseline conditions. The model, as presented here, provides a means to explore theories and mathematical representations of hydrophysical processes that drive or limit riparian seedling recruitment. Additionally, these models can be used to ask more exploratory questions that help improve understanding of how relevant processes interact and impact a system (Coulthard & Van De Wiel, 2013).

The underlying assumptions and differences between previously developed mechanistic models of riparian seedling recruitment potential were examined. Several limitations of previous models were identified, many of which were addressed in the development of our new riparian seedling recruitment model. Improvements include accounting for seedling mortality due to scour caused by sediment mobilization, the reduction of potential germination sites due to existing forest canopy, and the incorporation of substrate size data.

Performance of the newly developed model was tested for a set of 5 example flow records in a simple archetypal river channel geometry in order to facilitate comparison with the expected outcomes of each scenario. Expectations were based on a conceptual and quantitative understanding of how hydrophysical processes both drive and limit riparian seedling recruitment potential. All expected outcomes were accurately reflected in the corresponding model results, verifying that this model was implemented as intended and described. Verification of implementation is a critical step in ensuring the quality and structural realism of a model (Augusiak et al., 2014). The approach presented can be used as an example of a testable method to verify the implementation of a mechanistic potential niche model development without empirical data.

The development of documentation of model information and decision processes for transparency and benchmarking results has been identified as a good modeling practice that need more attention (Jakeman et al., 2024). This new model addresses limitations of existing models and removes barriers associated with issues of accessibility and transparency to provide an assessment method to predict seedling recruitment potential. The open-source nature of River Architect ensures that the model can be freely evaluated, modified, and applied by anyone with the necessary technical skills. This also improves reproducibility by providing a fully automated tool with detailed documentation and a full dataset that can be used for benchmarking. This model provides a generalized starting point for theoretical hypothesis testing and for further evaluation using site- and species-specific field data. Useful applications for this tool include creating predictions to test hypotheses, guiding observational campaigns, and comparing restoration or management alternatives.

Funding sources

This research was supported by the Yuba Water Agency (Marysville, California, USA; Award #201016094) and the USDA National Institute of Food and Agriculture (Hatch project number CA-D-LAW-7034-H). This research also benefited from a research scholarship from the Santa Clara Valley Chapter of the California Native Plant Society and a fellowship from the Henry A. Jastro and Peter J. Shields Endowments awarded to Sierra J. Phillips.

CRediT authorship contribution statement

Sierra J. Phillips: Writing – review & editing, Writing – original draft, Visualization, Validation, Software, Methodology, Investigation, Formal analysis, Conceptualization. **Gregory B. Pasternack:** Writing – review & editing, Supervision, Project administration, Methodology, Funding acquisition, Conceptualization. **Kenneth Larrieu:** Writing – review & editing, Visualization, Software, Methodology, Conceptualization.

Declaration of competing interest

The authors declare that they have no known competing financial interests or personal relationships that could have appear to influence the work reported in this paper.

Acknowledgements

We thank Sebastien Schwindt for creating the foundation on which this model could be built, River Architect. We thank Rachel Wright, Romina Diaz-Gomez, Yufang Jin, Mary Cadenasso, Paul Bratovich, Morgan Neil, Bryan Poxon, Geoff Rabone, and Jacob Vander Meulen for discussions about the model and riparian vegetation during model development.

Supplementary materials

Supplementary material associated with this article can be found, in the online version, at doi:10.1016/j.ecolmodel.2024.110986.

Data availability

This publication presents a literature review, model development, model testing with a canonical test channel, and a real-world example. Conforming to open-source standards, the code is available to the public at https://riverarchitect.github.io/. The archetype rasters and flow records for the five hydrologic scenarios are provided as part of the GitHub repository. River Architect has a DOI with Zenodo (https://zenodo.org/doi/10.5281/zenodo.3385164). For the real-world example, the proprietary data belongs to Yuba Water and can be requested of them through the senior author.

References

Amlin, N.A., Rood, S.B., 2001. Inundation tolerances of riparian willows and cottonwoods. J. Am. Water Resour. Assoc. 37 (6), 1709–1720. https://doi.org/10.1111/j.1752-1688.2001.tb03671.x.

Amlin, N.M., Rood, S.B., 2002. Comparative tolerances of riparian willows and cottonwoods to water-table decline. Wetl 22 (2), 338–346. https://doi.org/10.1672/0277-5212(2002)022[0338:CTORWA]2.0.CO;2.

Abu-Aly, T.R., Pasternack, G.B., Wyrick, J.R., Barker, R., Massa, D., Johnson, T., 2014. Effects of LiDAR-derived, spatially distributed vegetation roughness on two-dimensional hydraulics in a gravel-cobble river at flows of 0.2 to 20 times bankfull. Geomorphology 206, 468–482. https://doi.org/10.1016/J.GEOMORPH.2013.10.017.

Auchincloss, L.C., Richards, J.H., Young, C.A., Tansey, M.K., 2012. Inundation depth, duration, and temperature influence fremont cottonwood (Populus fremontii) seedling growth and survival. West. North Am. Nat. 72 (3), 323–333. https://doi.org/10.3398/064.072.0306.

Augusiak, J., Van den Brink, P.J., Grimm, V., 2014. Merging validation and evaluation of ecological models to "evaludation": a review of terminology and a practical approach. Ecol. Model. 280, 117–128. https://doi.org/10.1016/j.ecolmodel.2013.11.009.

Baker, W.L., 1990. Climatic and hydrologic effects on the regeneration of Populus angustifolia James along the Animas River. Colorado. J. Biogeog. 17 (1), 59. https://doi.org/10.2307/2845188.

Benjankar, R., Burke, M., Yager, E., Tonina, D., Egger, G., Rood, S.B., Merz, N., 2014. Development of a spatially-distributed hydroecological model to simulate cottonwood seedling recruitment along rivers. J. Environ. Manag. 145, 277–288. https://doi.org/10.1016/j.jenvman.2014.06.027.

Benjankar, R., Tranmer, A.W., Vidergar, D., Tonina, D., 2020. Riparian vegetation model to predict seedling recruitment and restoration alternatives. J. Environ. Manag. 276. https://doi.org/10.1016/j.jenvman.2020.111339.

BMT-WBM. (2018). TUFLOW Classic/HPC User Manual Build 2018-03-AD. 723.

Braatne, J.H., Jamieson, R., Gill, M., Rood, S.B., 2007. Instream flows and the decline of riparian cottonwoods along the Yakima River, Washington, USA. River Res. Appl. 23, 247–267. https://doi.org/10.1002/rra.978.

Burke, M., Jorde, K., Buffington, J.M., 2009. Application of a hierarchical framework for assessing environmental impacts of dam operation: changes in streamflow, bed mobility and recruitment of riparian trees in a western North American river. J. Environ. Manag. 90, S224–S236. https://doi.org/10.1016/j.jenvman.2008.07.022.

Bywater-Reyes, S., Wilcox, A.C., Stella, J.C., Lightbody, A.F., 2015. Flow and scour constraints on uprooting of pioneer woody seedlings. Water Resour. Res. 51 (11), 9190–9206. https://doi.org/10.1002/2014WR016641.

Caradima, B., Scheidegger, A., Brodersen, J., Schuwirth, N., 2021. Bridging mechanistic conceptual models and statistical species distribution models of riverine fish. Ecol. Model. 457 (June), 109680. https://doi.org/10.1016/j.ecolmodel.2021.109680.

Christensen, C., Katz, G., Friedman, J., Redmond, M.D., Norton, A., 2023. No evidence for cottonwood forest decline along a flow-augmented western U.S. river. River Res. App. 1–14. https://doi.org/10.1002/rra.4151.

Conard, S., MacDonald, R., Holland, R., 1977. Riparian vegetation and flora of the Sacramento Valley. In: Sands, A. (Ed.), Riparian Forests in California: Their Ecology and Conservation (47–55). Institute of Ecology Pub, No.15, University of California Davis, p. 122.

Cooke, J.E.K., Rood, S.B., 2007. Trees of the people: the growing science of poplars in Canada and worldwide. Canad. J. Bot. 85 (12), 1103–1110. https://doi.org/10.1139/B07-125.

Cooper, D.J., Andersen, D.C., Chimner, R.A., 2003. Multiple pathways for woody plant establishment on floodplains at local to regional scales. J. Ecol. 91 (2), 182–196. https://doi.org/10.1046/J.1365-2745.2003.00766.X.

Cooper, D.J., Merritt, D.M., Andersen, D.C., Chimner, R.A., 1999. Factors controlling the establishment of Fremont cottonwood seedlings on the upper Green River. USA. River Res. App. 15 (5), 419–440.

Coulthard, T.J., & Van De Wiel, M.J. (2013). Numerical modeling in fluvial geomorphology. In J.F. Shroder (Ed.), Treatise On Geomorphology (Vol. 9, 694–710). Academic Press. https://doi.org/10.1016/B978-0-12-374739-6.00261-X.

Díaz Gómez, R., Pasternack, G.B., Guillon, H., Byrne, C.F., Schwindt, S., Larrieu, K.G., Solis, S.S., 2022. Mapping subaerial sand-gravel-cobble fluvial sediment facies using airborne lidar and machine learning. Geomorphology 401, 108106. https://doi.org/10.1016/j.geomorph.2021.108106.

Dixon, M.D., 2003. Effects of Flow Pattern of Riparian Seedling Recruitment On Sandbars in the Wisconsin River, Wisconsin, USA. Springer Nature: Wetlands 23, 125–139. https://doi.org/10.1672/0277-5212(2003)023[0125:EOFPOR]2.0.CO;2.

Dixon, M.D., Johnson, W.C., Scott, M.L., Bowen, D.E., Rabbe, L.A., 2012. Dynamics of plains cottonwood (Populus deltoides) forests and historical landscape change along unchannelized segments of the Missouri River. USA. Environ. Manag. 49, 990–1008. https://doi.org/10.1007/s00267-012-9842-5.

Dixon, M.D., Turner, M.G., 2006. Simulated recruitment of riparian trees and shrubs under natural and regulated flow regimes on the Wisconsin River. USA. River Res. App. 22, 1057–1083. https://doi.org/10.1002/rra.948.

Du Boys, P., 1879. Le Rhône et Les Rivières à Lit Affouillable – Étude Du Régime Du Rhône et de L'action Exercée Par Les Eaux Sur Un Lit à Fond de Graviers Indéfiniment Affouillable. Annales Des Ponts et Chaussées, 49, 141–195.

Edmaier, K., Burlando, P., Perona, P., 2011. Mechanisms of vegetation uprooting by flow in alluvial non-cohesive sediment. Hydrol. Earth Syst. Sci. 15 (5), 1615–1627. https://doi.org/10.5194/hess-15-1615-2011.

Einstein, H.A., 1950. The Bed-Load Function for Sediment Transportation in Open Channel Flows. Techn. Bull. USDA Soil Conserv. Serv. 1026, 1–31.

Eriksson, O., Ehrlén, J., 2008. Seedling recruitment and population ecology. In: Leck, M. A., Parker, V.T., Simpson, R.L. (Eds.), Seedling Ecol. Evol. Cambridge University Press, pp. 239–254. https://doi.org/10.1017/CBO9780511815133.013.

Fitz, H.C., DeBellevue, E.B., Costanza, R., Boumans, R., Maxwell, T., Wainger, L., Sklar, F. H., 1996. Development of a general ecosystem model for a range of scales and ecosystems. Ecol. Model. 88 (1–3), 263–295. https://doi.org/10.1016/0304-3800(95)00112-3.

Harris, R.R., 1987. Occurrence of vegetation on geomorphic surfaces in the active floodplain of a California alluvial stream. Am. Midl. Nat. 118 (2), 393–405. https://doi.org/10.2307/2425796.

Holstein, G., 1984. California riparian forests. In: Warner, R.E., Hendrix, K.M. (Eds.), California Riparian Systems: Ecology, Conservation, and Productive Management. University of California Press, Berkeley, p. c1984.

Horemans, D.M.L., Friedrichs, M.A.M., St-Laurent, P., Hood, R.R., Brown, C.W., 2024. Evaluating the skill of correlative species distribution models trained with mechanistic model output. Ecol. Model. 491 (March), 110692. https://doi.org/10.1016/j.ecolmodel.2024.110692.

Howe, W.H., Knopf, F.L., 1991. On the imminent decline of Rio Grande cottonwoods in central New Mexico. Southwest. Nat. 36 (2), 218–224. https://doi.org/10.2307/3671924.

Hultine, K.R., Allan, G.J., Blasini, D., Bothwell, H.M., Cadmus, A., Cooper, H.F., Doughty, C.E., Gehring, C.A., Gitlin, A.R., Grady, K.C., Hull, J.B., Keith, A.R., Koepke, D.F., Markovchick, L., Corbin Parker, J.M., Sankey, T.T., Whitham, T.G., 2020. Adaptive capacity in the foundation tree species *Populus fremontii*: implications for resilience to climate change and non-native species invasion in the American Southwest. Conserv. Physiol. 8 (1), 1–16. https://doi.org/10.1093/conphys/coaa061.

Jakeman, A.J., Elsawah, S., Wang, H.-H., Hamilton, S.H., Melsen, L., Grimm, V., 2024. Towards normalizing good practice across the whole modeling cycle: its instrumentation and future research topics. Soc.-Environ. Syst. Model. 6, 18755. https://doi.org/10.18174/sesmo.18755.

Johnson, W.C., 1994. Woodland expansion in the Platte River, Nebraska: patterns and Causes. Ecol. Monogr. 64 (1), 45–84. https://doi.org/10.2307/2937055.

Johnson, W.C., 2000. Tree recruitment and survival in rivers: influence of hydrological process. Hydrol. Process. 14, 3051–3074. https://doi.org/10.1002/1099-1085(200011/12)14:16/17<3051::AID-HYP134>3.0.CO;2-1.

Kalischuk, A.R., Rood, S.B., Mahoney, J.M., 2001. Environmental influences on seedling growth of cottonwood species following a major flood. For. Ecol. Manag. 144 (1–3), 75–89. https://doi.org/10.1016/S0378-1127(00)00359-5.

Katibah, E.F., 1984. A Brief History of Riparian Forests in the Central Valley of California. In: Warner, R.E., Hendrix, K.M. (Eds.), California Riparian Systems: Ecology, Conservation, and Productive Management. University of California Press, Berkeley, p. c1984..

Keulegan, G.H., 1938. Laws of Turbulent Flow in Open Channels, 21. National Bureau of Standards.

Kozlowski, T.T., 2002. Physiological-ecological impacts of flooding on riparian forest ecosystems. Wetl 22, 550–561. https://doi.org/10.1672/0277-5212(2002)022[0550:PEIOFO]2.0.CO;2.

Kramer, H., 1932. Modellgeschiebe Und Schleppkraft [Modelling bed Load and Drag Force]. Preußische Versuchsanstalt Für Wasserbau Und Schiffbau.

Kui, L., Stella, J.C., 2016. Fluvial sediment burial increases mortality of young riparian trees but induces compensatory growth response in survivors. For. Ecol. Manag. 366, 32–40. https://doi.org/10.1016/J.FORECO.2016.02.001.

Lamb, M.P., Dietrich, W.E., Venditti, J.G., 2008. Is the critical shields stress for incipient sediment motion dependent on channel-bed slope? J. Geophys. Res.: Earth Surf. 113 (2). https://doi.org/10.1029/2007JF000831.

Larrieu, K.G., Pasternack, G.B., Schwindt, S., 2021. Automated analysis of lateral river connectivity and fish stranding risks—part 1: review, theory and algorithm. Ecohydrology 14 (2), e2268. https://doi.org/10.1002/ECO.2268.

Li, T., Pasternack, G.B., 2023. Applying flow convergence routing to control sediment erosion and deposition locations in a dam's backwater zone. Geomorphology 440, 108882. https://doi.org/10.1016/J.GEOMORPH.2023.108882.

Lytle, D.A., Merritt, D.M., 2004. Hydrologic regimes and riparian forests: a structured population model for cottonwood. Ecol 85 (9), 2493–2503. https://doi.org/10.1890/04-0282.

Mahoney, J.M., Rood, S.B., 1998. Streamflow requirements for cottonwood seedling recruitment - an integrative model. Wetl 18 (4), 634–645. https://doi.org/10.1007/BF03161678.

Neuman, D.S., Wagner, M., Braatne, J.H., Howe, J., 1996. Stress physiology—abiotic. In: Stettler, R.F., Bradshaw, H.D., Heilman, P.F., Hinckley, T.M. (Eds.), Biology of *Populus* and Its Implications for Management and Conservation. NRC Research Press, pp. 423–449.

Nilsson, C., Berggren, K., 2000. Alterations of riparian ecosystems caused by river regulation. BioSci 50 (9), 783–792. https://doi.org/10.1641/0006-3568(2000)050[0783:AORECB]2.0.CO;2.

Oreskes, N., Belitz, K., 2001. Philosophical issues in model assessment. Model Valid. 23. January 2001.

Pasternack, G.B., 2011. 2D Modeling and Ecohydraulic Analysis. Createspace.

Pasternack, G.B., 2023. 2017 Lower Yuba River TUFLOW HPC 2D Model Description, Validation, and Exploratory Simulations. Prepared for Yuba Water Agency.

Perry, L.G., Shafroth, P.B., Hay, L.E., Markstrom, S.L., Bock, A.R., 2020. Projected warming disrupts the synchrony of riparian seed release and snowmelt streamflow. New Phytol. 225 (2), 693–712. https://doi.org/10.1111/NPH.16191.

Peterson, A.T., Papeş, M., Soberón, J., 2015. Mechanistic and correlative models of ecological niches. Eur. J. Ecol. 1 (2), 28–38. https://doi.org/10.1515/eje-2015-0014.

Philipsen, L.J., Romuld, M.A., Rood, S.B., 2021. Floodplain forest dynamics: half-century floods enable pulses of geomorphic disturbance and cottonwood colonization along a prairie river. River Res. App. 37 (1), 64–77. https://doi.org/10.1002/rra.3740.

Philipsen, L.J., Rood, S.B., 2022. Riparian recruitment persists after damming: environmental flows and coupled colonization of cottonwoods and willows following floods along a dryland river. River Res. App. 38 (9), 1642–1653. https://doi.org/10.1002/rra.4030.

Poff, N.L.R., 1997. Landscape filters and species traits: towards mechanistic understanding and prediction in stream ecology. J. North Am. Benthol. Soc. 16 (2), 391–409. https://doi.org/10.2307/1468026.

Read, R.A., 1958. Silvical characteristics of plains cottonwood. USDA For. Serv., Rocky Mountain Forest and Range Experiment Station Paper Number 33.

Ribbens, E., Silander Jr., J.A., Pacala, S.W., 1994. Seedling recruitment in forests: calibrating models to predict patterns of tree seedling dispersion. Ecol 75 (6), 1794–1806. https://doi.org/10.2307/1939638.

Rickenmann, D., Recking, A., 2011. Evaluation of flow resistance in gravel-bed rivers through a large field data set. Water Resour. Res. 47 (7). https://doi.org/10.1029/2010WR009793.

Rood, S.B., Goater, L.A., Mahoney, J.M., Pearce, C.M., Smith, D.G., 2007. Floods, fire, and ice: disturbance ecology of riparian cottonwoods. Canad. J. Bot. 85, 1019–1032. https://doi.org/10.1139/B07-073.

Rood, S.B., Gourley, C.R., Ammon, E.M., Heki, L.G., Klotz, J.R., Morrison, M.L., Mosley, D., Scoppetttone, G.G., Swanson, S., Wagner, P.L., 2003. Flows for floodplain forests: a successful riparian restoration. BioSci 53 (7), 647–656. https://doi.org/10.1641/0006-3568(2003)053[0647:FFFFAS]2.0.CO;2.

Rood, S.B., Heinze-Milne, S., 1989. Abrupt downstream forest decline following river damming in southern Alberta. Canad. J. Bot. 67 (6), 1744–1749. https://doi.org/10.1139/b89-221.

Rood, S.B., Kalischuk, A.R., Mahoney, J.M., 1998. Initial cottonwood seedling recruitment following the flood of the century of the Oldman River. Canada. Wetl. 18, 557–570. https://doi.org/10.1007/BF03161672.

Rood, S.B., Mahoney, J.M., 1990. Collapse of riparian poplar forests downstream from dams in western prairies: probable causes and prospects for mitigation. Environ. Manag. 14, 451–464. https://doi.org/10.1007/BF02394134.

Rood, S.B., Mahoney, J.M., 2000. Revised Instream Flow Regulation Enables Cottonwood Recruitment Along the St. Mary River. Rivers 7 (2), 109–125.

Sawyer, A.M., Pasternack, G.B., Moir, H.J., Fulton, A.A., 2010. Riffle-pool maintenance and flow convergence routing observed on a large gravel-bed river. Geomorphology 114 (3), 143–160. https://doi.org/10.1016/j.geomorph.2009.06.021.

Schwindt, S., Larrieu, K., Pasternack, G.B., & Rabone, G. (2020). River Architect. SoftwareX, 11. https://doi.org/10.1016/j.softx.2020.100438.

Schwindt, S., Pasternack, G.B., Bratovich, P.M., Rabone, G., Simodynes, D., 2019. Hydro-morphological parameters generate lifespan maps for stream restoration management. J. Environ. Manag. 232, 475–489. https://doi.org/10.1016/j.jenvman.2018.11.010.

Scott, M.L., Friedman, J.M., Auble, G.T., 1996. Fluvial process and the establishment of bottomland trees. Geomorphology 14 (4), 327–339. https://doi.org/10.1016/0169-555X(95)00046-8.

Scott, M.L., Miller, M.E., 2017. Long-term cottonwood establishment along the Green River, Utah, USA. Ecohydrology 10 (3), 1–11. https://doi.org/10.1002/eco.1818.

Shafroth, P.B., Auble, G.T., Scott, M.L., 1995. Germination and establishment of the native plains cottonwood (*Populus deltoides Marshall subsp. monilifera*) and the exotic Russian-olive (*Elaeagnus angustifolia L.*). Conserv. Biol. 9 (5), 1169–1175. https://doi.org/10.1046/j.1523-1739.1995.9051159.x-i1.

Shafroth, P.B., Auble, G.T., Stromberg, J.C., Patten, D.T., 1998. Establishment of woody riparian vegetation in relation to annual patterns of streamflow, Bill Williams River, Arizona. Wetl 18, 577–590. https://doi.org/10.1007/BF03161674.

Shields, A., 1936. Anwendung Der Aehnlichkeitsmechanik und Der Turbulenzforschung auf Die Geschiebebewegung [Application of Similarity Mechanics and Turbulence Research On Shear Flow], 26. Mitteilungen der Preußischen Versuchsanstalt für Wasserbau.

Sillero, N., 2011. What does ecological modelling model? A proposed classification of ecological niche models based on their underlying methods. Ecol. Model. 222 (8), 1343–1346. https://doi.org/10.1016/j.ecolmodel.2011.01.018.

Silva, P.V., Pasternack, G.B., 2018. 2017 Lower Yuba River Topographic Mapping Report. Prepared for the Yuba Water Agency.

Singer, A., Johst, K., Banitz, T., Fowler, M.S., Groeneveld, J., Gutiérrez, A.G., Hartig, F., Krug, R.M., Liess, M., Matlack, G., Meyer, K.M., Pe'er, G., Radchuk, V., Voinopol-Sassu, A.J., Travis, J.M.J., 2016. Community dynamics under environmental change: how can next generation mechanistic models improve projections of species distributions? Ecol. Model. 326, 63–74. https://doi.org/10.1016/j.ecolmodel.2015.11.007.

Stanford, J.A., Lorang, M.S., Hauer, F.R., 2005. The shifting habitat mosaic of river ecosystems. Internationale Vereinigung Für Theoretische Und Angewandte Limnologie: Verhandlungen 29 (1), 123–136. https://doi.org/10.1080/03680770.2005.11901979.

Stella, J.C., 2005. A Field-Calibrated Model of Pioneer Riparian Tree Recruitment For the San Joaquin Basin. CA [Dissertation]. University of California, Berkeley.

Stella, J.C., Battles, J.J., McBride, J.R., Orr, B.K., 2010. Riparian seedling mortality from simulated water table recession, and the design of sustainable flow regimes on regulated rivers. Restor. Ecol. 18, 284–294. https://doi.org/10.1111/j.1526-100X.2010.00651.x.

Stella, J.C., Battles, J.J., Orr, B.K., McBride, J.R., 2006. Synchrony of seed dispersal, hydrology and local climate in a semi-arid river reach in California. Ecosyst. 9, 1200–1214. https://doi.org/10.1007/s10021-005-0138-y.

Stella, J.C., Bendix, J., 2019. Chapter 5 - Multiple stressors in riparian ecosystems. In: Sabater, S., Elosegi, A., Ludwig, R. (Eds.), Multiple Stressors in River Ecosystems: Status, Impacts and Prospects for the Future, pp. 81–110. https://doi.org/10.1016/B978-0-12-811713-2.00005-4.

Strahan, J., 1984. Regeneration of riparian forests of the Central Valley. California Riparian Systems: Ecology, Conservation, and Productive Management. University of California Press, Berkeley, pp. 58–67.

Stromberg, J.C., 1993. Fremont cottonwood-goodding willow riparian forests: a review of their ecology, threats, and recovery potential. J. Ariz.-Nev. Ac. Sci. 27 (1), 97–110.

Stromberg, J.C., Patten, D.T., Richter, B.D., 1991. Flood flows and dynamics of Sonoran riparian forests. Rivers 2 (3), 221–235.

Tranmer, A.W., Benjankar, R., Vidergar, D., Tonina, D., 2023. Identifying failure mechanisms of native riparian forest regeneration in a variable-width floodplain using a spatially-distributed riparian forest recruitment model. Ecol. Eng. 187, 106865. https://doi.org/10.1016/j.ecoleng.2022.106865.

Tucker, G., Lancaster, S., Gasparini, N., Bras, R., 2001. The Channel-Hillslope integrated landscape development model (CHILD). In: Doe, R.S. (Ed.), Lands Erosion and Evolution Modeling. Springer, Boston, MA. https://doi.org/10.1007/978-1-4615-0575-4_12.

USACE. (2012). Lower Yuba river large woody material management plan pilot study (Issue August).

USACE. (2014). Yuba river ecosystem restoration section 905 (b) analysis (Issue October).

Vesipa, R., Camporeale, C., Ridolfi, L., 2017. Effect of river flow fluctuations on riparian vegetation dynamics: processes and models. Adv. Water Resour. 110, 29–50. https://doi.org/10.1016/J.ADVWATRES.2017.09.028.

Von Karmàn, T., 1930. Mechanical similarity and turbulence. In: Third International Congress for Applied Mechanics, pp. 79–93.

Wang, J., Zhang, Z., Greimann, B., Huang, V., 2018. Application and evaluation of the HEC-RAS – riparian vegetation simulation module to the Sacramento River. Ecol. Model. 368, 158–168. https://doi.org/10.1016/J.ECOLMODEL.2017.11.011.

Williams, J., Stella, J.C., Voelker, S.L., Lambert, A.M., Pelletier, L.M., Drake, J.E., Friedman, J.M., Roberts, D.A., Singer, M.B., 2022. Local groundwater decline exacerbates response of dryland riparian woodlands to climatic drought. Glob. Chang. Biol. 28 (22), 6771–6788. https://doi.org/10.1111/GCB.16376.

Wyrick, J.R., Pasternack, G.B., 2014. Geospatial organization of fluvial landforms in a gravel-cobble river: beyond the riffle-pool couplet. Geomorphology 213, 48–65. https://doi.org/10.1016/j.geomorph.2013.12.040.